Research Paper

GEOSPHERE

GEOSPHERE

https://doi.org/10.1130/GES02510.1

11 figures; 1 table; 1 set of supplemental files

CORRESPONDENCE: lberanek@mun.ca

CITATION: van Drecht, L.H., Beranek, L.P., Colpron, M., and Wiest, A.C., 2022, Development of the Whitehorse trough as a strike-slip basin during Early to Middle Jurassic arc-continent collision in the Canadian Cordillera: Geosphere, https://doi.org/10.1130/GES02510.1.

Science Editor: Christopher J. Spencer
Associate Editor: Joel Saylor

Received 29 December 2021
Revision received 27 April 2022
Accepted 2 June 2022

Published online 11 August 2022

Development of the Whitehorse trough as a strike-slip basin during Early to Middle Jurassic arc-continent collision in the Canadian Cordillera

Leigh H. van Drecht[1], Luke P. Beranek[1], Maurice Colpron[2], and Adam C. Wiest[1]

[1]Department of Earth Sciences, Memorial University of Newfoundland, 9 Arctic Avenue, St. John's, Newfoundland and Labrador A1B 3X5, Canada
[2]Yukon Geological Survey, P.O. Box 2703 (K14), Whitehorse, Yukon Y1A 2C6, Canada

ABSTRACT

The Whitehorse trough is a synorogenic basin in the northern Cordillera that resulted from arc-collision processes along the northwestern margin of North America, but its filling history and tectonic significance remain uncertain. New detrital zircon U-Pb-Hf isotope analyses of 12 rock samples, including six basal sandstones that sit unconformably on Triassic rocks of Stikinia, were combined with published detrital zircon and fossil data to establish the depositional ages of synorogenic Laberge Group strata in Yukon and test proposed links between Intermontane terrane exhumation and basin-filling events. Laberge Group strata yielded 205–170 Ma and 390–252 Ma detrital zircon populations that indicate derivation from local Late Triassic to Middle Jurassic arc and syncollisional plutons and metamorphosed Paleozoic basement rocks of the Stikinia and Yukon-Tanana terranes. Basal sandstone units have Early Jurassic depositional ages that show the Whitehorse trough filled during early Sinemurian, late Sinemurian to Pliensbachian, and Toarcian subsidence events. Late Triassic to Early Jurassic detrital zircon grains confirm that syncollisional plutons near the northern trough were exhumed at 0.5–7.5 mm/yr and replicate their excursion to subchondritic Hf isotope compositions as a result of increasing crustal contributions from Rhaetian to Sinemurian time. The new detrital zircon data, combined with recent constraints for Triassic–Jurassic metamorphism and magmatism in Yukon, require modification of published forearc to syncollisional basin models for the Whitehorse trough. We reinterpret Jurassic subsidence patterns and architecture of the Whitehorse trough to reflect sinistral transtension within a transform fault system that resulted from the reorganization of subduction after end-on arc collision.

INTRODUCTION

Synorogenic strata are the depositional records of mountain building and provide opportunities to investigate the timing of plate-tectonic processes along convergent margins. Immature terrestrial and marine siliciclastic strata in orogen-proximal basins have provenance signatures that faithfully record regional geology (Dickinson and Suczek, 1979; Dickinson et al., 1983; Ingersoll et al., 1993; Johnsson, 1993; Link et al., 2005) and are generated in response to discrete crustal thickening, exhumation, and other convergent margin events (e.g., Dickinson, 1974; Cawood et al., 2009, 2012; Horton, 2018; Enkelmann et al., 2019). Detrital zircon U-Pb isotope studies have proven to be useful for constraining the age, provenance, and paleogeography of ancient synorogenic rock units along Cordilleran-type margins, which are characterized by multiphase deformation, metamorphism, and magmatism (e.g., Willner et al., 2008; Amato and Pavlis, 2010; Horton et al., 2010; Wu et al., 2010; Anfinson et al., 2012; Laskowski et al., 2013; Beranek et al., 2016; Romero et al., 2020). Detrital zircon Hf isotope geochemistry has emerged as a complementary tool for identifying the crust-mantle contributions of igneous source rocks, and, as a result, it provides evidence for regional crustal evolution in the stratigraphic record (e.g., Hawkesworth and Kemp, 2006; Flowerdew et al., 2007; Iizuka et al., 2010; Liu et al., 2017). Detrital zircon U-Pb-Hf isotope investigations of synorogenic strata give opportunities to monitor increased crustal contributions during non-steady-state subduction or collisional events, which are typically defined by excursions toward subchondritic compositions or negative (evolved) $\varepsilon Hf_{(t)}$ values, known as isotopic pull-downs (DeCelles et al., 2009; DeCelles and Graham, 2015; Pecha et al., 2016).

The Intermontane terranes comprise the core of the Canadian Cordillera and are flanked to the east by parautochthonous units of the North American margin and to the west by the more exotic Insular and Alaskan terranes (Fig. 1; e.g., Mortensen, 1992; Monger and Price, 2002; Colpron et al., 2007a; Nelson et al., 2013). The Late Triassic to Middle Jurassic (all stratigraphic and numerical ages follow the time scale of Cohen et al., 2013) tectonic evolution of the northern Canadian Cordillera was marked by waning arc magmatism, arc collision, syn- to postcollisional magmatism, and syntectonic filling of the Whitehorse trough, which overlaps Upper Triassic and older rocks of the Stikinia and Cache Creek terranes from central Yukon to northern British Columbia (Figs. 1 and 2; e.g., Mihalynuk et al., 1994; English and Johnston, 2005; Colpron et al., 2015, 2022). Late Triassic to Middle Jurassic arc collision was accommodated by

Luke Beranek https://orcid.org/0000-0003-3086-7935

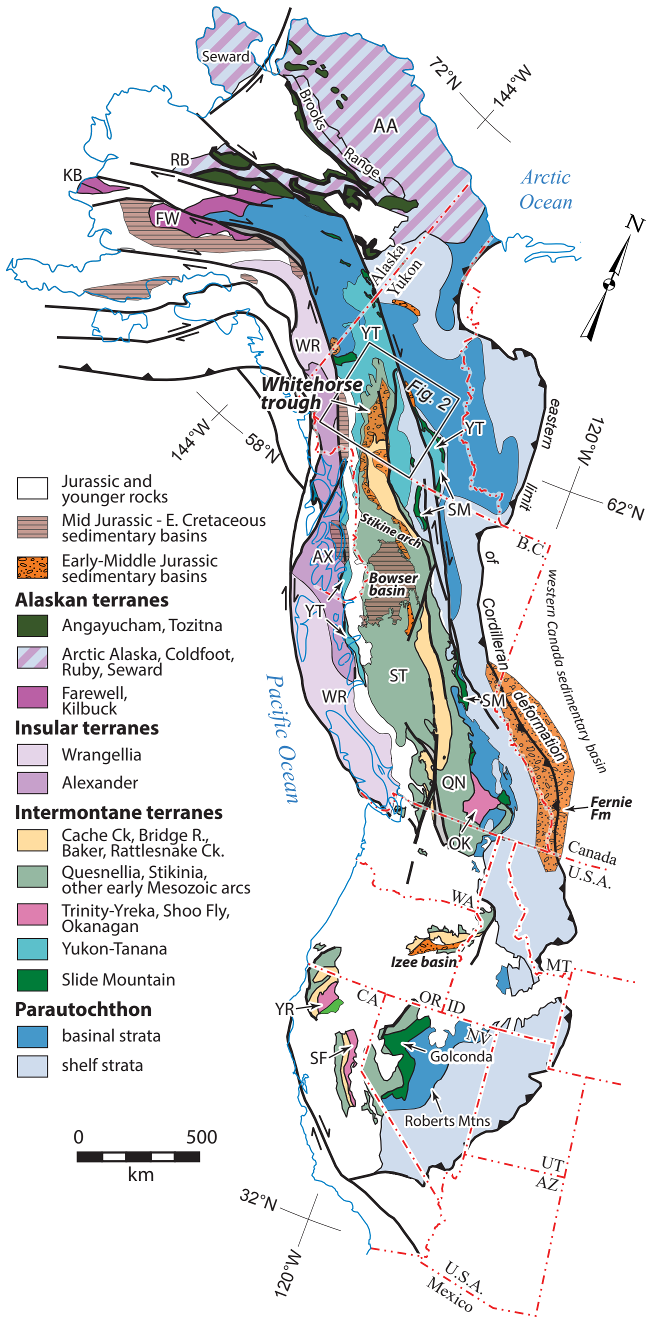

the enclosure of the Cache Creek terrane and resulted in crustal thickening and burial of Yukon-Tanana terrane rocks to 5–9 kbar (~16–30 km) in Yukon (e.g., Berman et al., 2007; Clark, 2017; Gaidies et al., 2021). Late Triassic to Early Jurassic (205–194 Ma) syncollisional plutons were emplaced at mid- to lower-crustal levels (5–7 kbar, ~16–23 km) into metamorphic basement along the flanks of the Whitehorse trough and subsequently cooled and exhumed at rates of 0.7–7.5 mm/yr (e.g., Johnston and Erdmer, 1995; Johnston et al., 1996; Knight et al., 2013; Colpron et al., 2022). Exhumation processes in central Yukon drove Early to Middle Jurassic erosion and resulted in the syntectonic deposition of the Laberge Group, a >3000-m-thick succession of immature marginal-marine to deep-marine strata that are typically interpreted to have filled a forearc basin (e.g., Dickie and Hein, 1995; English and Johnston, 2005) or a syncollisional basin that overlapped the northern Intermontane terranes (Colpron et al., 2015). Recently, Colpron et al. (2022) proposed that latest Triassic to Early Jurassic end-on arc collision in the northern Intermontane terranes was followed by southward migration of the Stikinia arc (Hazelton Group; Nelson et al., 2022) and that the collision zone in the north was linked to the retreating subduction zone by a sinistral transform fault system, possibly including the Llewellyn and Teslin faults (Currie and Parrish, 1993; Mihalynuk et al., 1999; de Keijzer et al., 2000). This new model predicts that sinistral transtension accommodated extensional exhumation of the orogen and subsidence of the Whitehorse trough as a strike-slip basin. Basal units of the Laberge Group are lithologically diverse and overlie different sedimentary and igneous rock substrates in Yukon (Lowey, 2004; Colpron et al., 2007b), which together imply block-faulted basement topography and multiple erosion-deposition events during Whitehorse trough subsidence. Laberge Group deposition was coeval with the onset of Jurassic foreland basin subsidence in Alberta (Fernie Formation in Fig. 1; Cant and Stockmal, 1989; Price, 1994; Pană et al., 2018) and suggests that the development of the Whitehorse trough accompanied the rise of the Cordilleran hinterland-retroarc thrust system (Colpron et al., 2015, 2022).

The timing of Laberge Group deposition and relative sediment contributions from Intermontane terrane sources during regional exhumation are required to understand the tectonic setting and filling history of the Whitehorse trough. In this article, we build on field studies (van Drecht et al., 2017; van Drecht and Beranek, 2018; Bordet et al., 2019) and report new detrital zircon U-Pb-Hf results from 12 Laberge Group sandstone samples, including six basal samples that sit unconformably on Triassic sedimentary and intrusive rocks of Stikinia. We

Figure 1. Paleozoic to early Mesozoic terranes of the North American Cordillera modified from Colpron and Nelson (2009). Terranes are grouped according to crustal affinity and interpreted positions in early Paleozoic time. Outlined box shows the geographic location of Whitehorse trough in Figure 2. Terrane abbreviations: AA—Arctic Alaska; AX—Alexander; FW—Farewell; KB—Kilbuck; OK—Okanagan; QN—Quesnellia; RB—Ruby; SF—Shoo Fly complex; SM—Slide Mountain; ST—Stikinia; WR—Wrangellia; YR—Yreka and Trinity; YT—Yukon-Tanana terrane. State and province abbreviations: AZ—Arizona, B.C.—British Columbia (Canada), CA—California, ID—Idaho, MT—Montana, NV—Nevada, OR—Oregon, UT—Utah, WA—Washington. Other abbreviations: Ck.—Creek; R.—River.

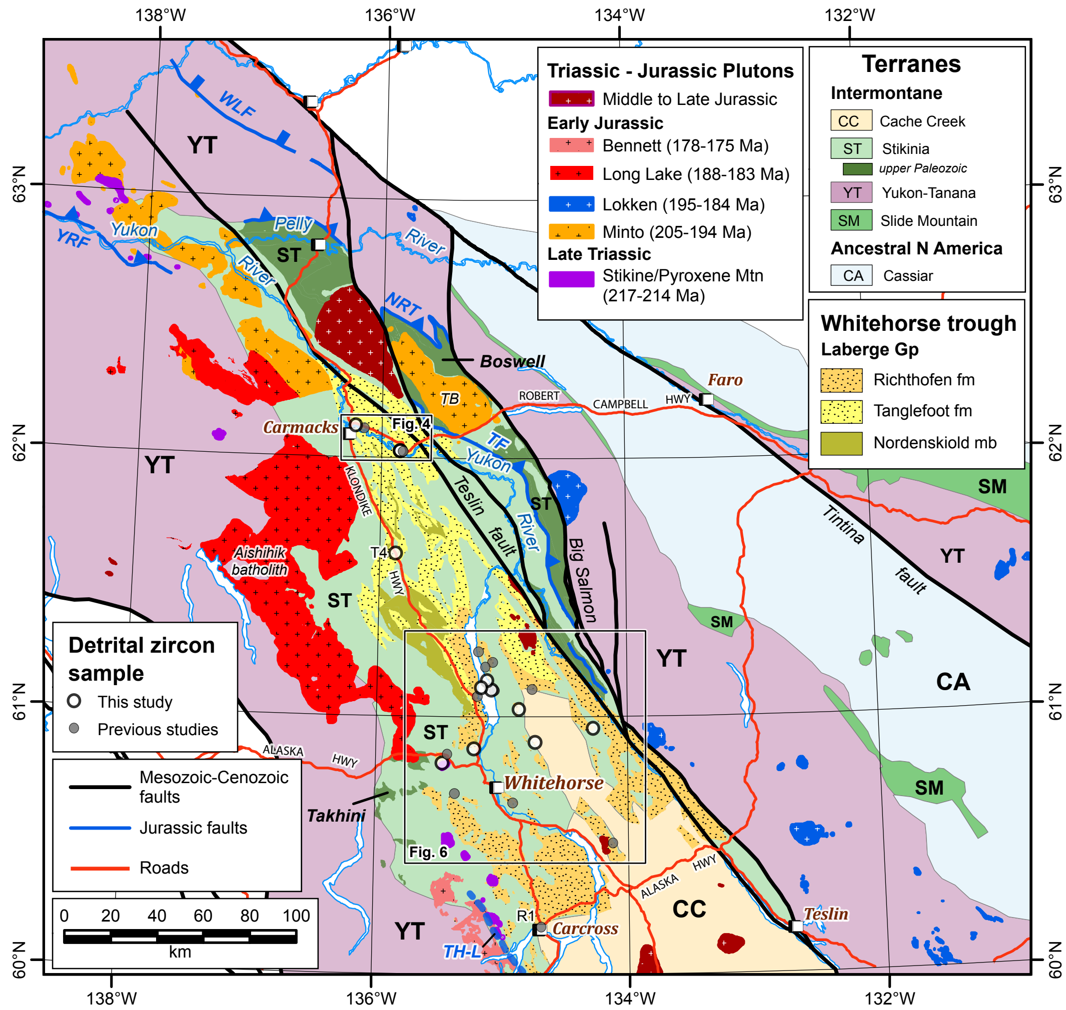

Figure 2. Simplified geologic map of the northern Intermontane terranes and Whitehorse trough in Yukon, Canada. The locations of detrital zircon samples analyzed for this and previous studies (Colpron et al., 2015; Bordet et al., 2019) are shown here and in detailed maps (Figs. 4 and 6). Jurassic faults are shown in blue: NRT—Needlerock thrust; TF—Tadru fault; TH-L—Tally Ho–Lewellyn faut zone; WLF—Willow Lake fault; YRF—Yukon River fault. Other abbreviations: TB—Tatchun batholith; fm—formation; mb—member.

used this data set to test the relationships between the timing of exhumation and Whitehorse trough deposition. The laser-ablation split-stream technique, which allows for the simultaneous collection of U-Pb and Hf isotope data in zircon (e.g., Fisher et al., 2014; Beranek et al., 2020), was used to identify juvenile to evolved source rocks and characterize an isotopic pull-down recorded by Laberge Group strata. This isotopic pattern matches the one recognized in syncollisional plutonic rocks that intruded the Intermontane terranes during an Early Jurassic episode of crustal thickening in the northern Canadian Cordillera (Colpron et al., 2022). We combined our new detrital zircon U-Pb-Hf isotope data with published fossil and U-Pb results (Colpron, 2011; Colpron et al., 2015; Bordet et al., 2019) to constrain Sinemurian to Toarcian maximum depositional ages for Laberge Group units and basin-filling patterns. These data suggest that the pattern of subsidence in the Whitehorse trough is consistent with development as a strike-slip basin within a sinistral transtensional regime during the early stages of development of the northern Cordilleran orogen (Colpron et al., 2022).

GEOLOGIC FRAMEWORK

The Intermontane realm of the Canadian Cordillera includes the Yukon-Tanana, Stikinia, and Quesnellia arc terranes and oceanic and accretionary complexes of the Slide Mountain and Cache Creek terranes (Fig. 1; e.g., Nelson et al., 2013). Late Devonian to late Permian arc successions of the Yukon-Tanana terrane intrude and cover the Snowcap assemblage, a metasedimentary basement unit that yields Precambrian detrital zircon age populations consistent with northwest Laurentian provenance (Mortensen, 1992; Colpron et al., 2006, 2007a; Piercey and Colpron, 2009). Development of the Yukon-Tanana arc occurred concurrently with rifting and opening of the Slide Mountain back-arc ocean between the Late Devonian and Permian (e.g., Nelson et al., 2006). The Yukon-Tanana terrane locally forms the depositional basement to the early Mesozoic Quesnellia arc in Yukon and British Columbia (e.g., Simard et al., 2003; Nelson and Friedman, 2004; Roots et al., 2006; Nixon et al., 2020; Colpron et al., 2022). Upper Paleozoic arc successions also form the basement to Triassic arc volcanic and sedimentary rocks of northern Stikinia, but their correlation with the Yukon-Tanana terrane is tenuous (e.g., George et al., 2021); they include the Stikine assemblage in northern British Columbia (e.g., Gunning et al., 2006) and the Takhini and Boswell assemblages in south-central Yukon (Fig. 2; Tempelman-Kluit, 1984; Hart, 1997; Colpron et al., 2006). Overlying Upper Triassic volcanic and sedimentary rocks of Stikinia and Quesnellia have similar stratigraphic and petrogenetic histories and are generally interpreted to have formed part of a single, continuous arc system that now occurs on either side of an accretionary complex and related oceanic rock units of the Cache Creek terrane (Fig. 1; Nelson and Mihalynuk, 1993; Mihalynuk et al., 1994).

Late Paleozoic to early Mesozoic collapse of the marginal ocean basin system along western Laurentia, the vestiges of which comprise the Slide Mountain terrane (Fig. 1), resulted in the docking of Yukon-Tanana and Quesnellia against the North American margin and deposition of Triassic overlap assemblages in eastern Alaska, Yukon, and British Columbia (Unterschutz et al., 2002; Beranek et al., 2010; Beranek and Mortensen, 2011; Golding et al., 2016). Stikinia was likely part of a west-facing arc festoon that protruded into Panthalassa, similar to the modern Aleutian arc, and flourished during the Middle to Late Triassic along western Pangea (e.g., Mihalynuk et al., 1994; George et al., 2021; Colpron et al., 2022). In south-central Yukon, Middle Triassic rocks of the Joe Mountain Formation include Ladinian basalt with tholeiitic arc to back-arc geochemical affinities, siliciclastic and calcareous strata, and mafic intrusions (Hart, 1997; Bordet et al., 2019; Bickerton et al., 2020). The Joe Mountain Formation has tentatively been assigned to Stikinia (e.g., Hart, 1997), but recent studies suggest it may be correlative with primitive arc successions assigned to the Cache Creek terrane in British Columbia (e.g., Kutcho-Nakina assemblages; Zagorevski et al., 2018; Bordet et al., 2019; Bickerton et al., 2020). Zagorevski et al. (2021) assigned these rocks to the newly defined Atlin terrane.

Upper Triassic strata of Stikinia in Yukon comprise the Lewes River Group (Fig. 3; Wheeler, 1961) and include: (1) Carnian volcaniclastic rocks and augite-phyric basalt of the Povoas formation (informal; Tempelman-Kluit,

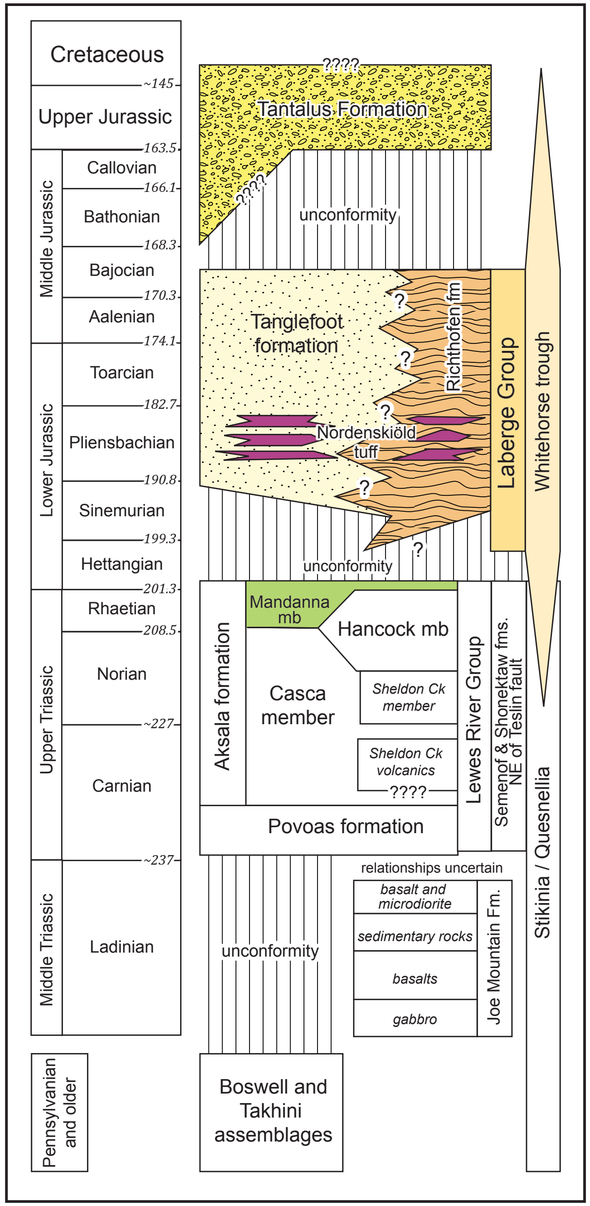

Figure 3. Upper Paleozoic–Mesozoic stratigraphic chart (with ages in Ma) for Stikinia, Quesnellia, and the Whitehorse trough in central Yukon modified from Hart (1997), Colpron et al. (2015), and Bordet et al. (2019). Abbreviations: fm.—formation; mb—member; Ck—Creek.

1984; Hart, 1997); and (2) Carnian to Rhaetian sedimentary rocks of the Aksala formation (informal; Tempelman-Kluit, 1984), which consists of the Casca, Hancock, and Mandanna members (Fig. 3). The Casca member contains Carnian to Norian lithic sandstone, argillite, and conglomerate units that are overlain by Norian to Rhaetian reefal limestone of the Hancock member (Hart, 1997; Bordet et al., 2019). Rhaetian sandstone, mudstone, and conglomerate units of the terrestrial to marginal-marine Mandanna member interfinger with and overlie the Hancock member (Tempelman-Kluit, 1984; Dickie and Hein, 1995; Hart, 1997; Long, 2005). The Aksala formation locally overlaps volcanic strata of the Joe Mountain and Povoas formations (Bordet et al., 2019). Augite-phyric basalt, volcaniclastic, and carbonate rocks of the Upper Triassic Semenof formation (informal; Tempelman-Kluit, 1984; Simard and Devine, 2003) are correlatives of the Lewes River Group to the east of the Teslin fault in central Yukon (Fig. 2).

Norian to Rhaetian arc plutons intrude Triassic volcanic assemblages of Stikinia (Stikine suite, 217–214 Ma; Headless plugs, 208–207 Ma) and Paleozoic basement of the Yukon-Tanana terrane (Pyroxene Mountain suite, 218–214 Ma; Fig. 2; Sack et al., 2020; Colpron et al., 2022). These arc plutons have juvenile whole-rock Nd-Sr and zircon Hf ($\varepsilon Hf_{[t]}$ = +9.7 to +11.5) isotope compositions that indicate depleted mantle sources with little to no crustal contamination.

LATE TRIASSIC TO JURASSIC TECTONICS AND MAGMATISM

The Whitehorse trough is located at the center of an inverted V-shaped map pattern shown by the northern Intermontane terranes in Yukon and British Columbia (Fig. 1), which has typically been explained by Late Jurassic to Early Cretaceous strike-slip duplication of the Stikinia-Quesnellia arc (Wernicke and Klepacki, 1988) or Late Triassic to Middle Jurassic oroclinal bending of the Stikinia-Quesnellia arc and entrapment of the oceanic Cache Creek terrane (Mihalynuk et al., 1994; Colpron et al., 2015). Colpron et al. (2022) proposed an alternative model where entrapment of the Cache Creek terrane resulted from development of a sinistral transform fault system linked to the southward retreat of an Early Jurassic arc (Hazelton Group; Nelson et al., 2022) following initial, latest Triassic collision. In this model, the Whitehorse trough developed atop of the northern Intermontane terranes within a sinistral transtensional setting in the collisional zone to the north (Colpron et al., 2015, 2022). The Cache Creek ocean was consumed by Middle Jurassic time (e.g., Cordey, 2020), and its oceanic assemblages were emplaced onto Stikinia along thrust faults, marking the accretion of the Intermontane terranes against the continental margin (Mihalynuk et al., 1994, 2004).

Hettangian to Sinemurian (ca. 200–190 Ma) prograde metamorphism and burial of Yukon-Tanana terrane basement rocks to midcrustal levels (5–9 kbar, amphibolite facies) in western Yukon constrain the onset of collisional tectonism in the northern Intermontane terranes (e.g., Johnston et al., 1996; Berman et al., 2007; Clark, 2017; Gaidies et al., 2021). This was accompanied by intrusion of latest Triassic to Early Jurassic syncollisional plutons (Minto suite, 205–194 Ma; Sack et al., 2020) in Stikinia and the Yukon-Tanana terrane of central Yukon (Fig. 2). The Minto suite includes large batholiths with metaluminous to peraluminous geochemical signatures and whole-rock Nd ($\varepsilon Nd_{[t]}$ = –3.6 to +1.3) and zircon Hf ($\varepsilon Hf_{[t]}$ = 0 to +5) isotope compositions that show a shift toward subchondritic values relative to Late Triassic arc successions (Colpron et al., 2022). Al-in-hornblende pressures of 5–7 kbar suggest emplacement at mid- to lower-crustal depths (Sack et al., 2020). Exhumation of the Yukon-Tanana terrane and Minto suite plutons began by the Pliensbachian and probably was accommodated by crustal-scale normal faults such as the Willow Lake fault in central Yukon (Fig. 2; Knight et al., 2013). The $^{40}Ar/^{39}Ar$ mica cooling dates from Minto plutons suggest exhumation rates of 1.3–7.5 mm/yr (assuming a geothermal gradient of 25–30 °C/km; Sack et al., 2020).

Plutons of the Long Lake (Pliensbachian, 188–183 Ma) and Bennett suites (Toarcian, 178–175 Ma) intruded the Yukon-Tanana–Stikinia boundary during regional exhumation of the western flank of the Whitehorse trough. Long Lake and Bennett suite plutons were emplaced at shallower crustal depths (4–6 kbar) compared to Minto plutons and have peraluminous geochemical signatures and more-evolved whole-rock Nd ($\varepsilon Nd_{[t]}$ = –5.9 to –1.5) and zircon Hf ($\varepsilon Hf_{[t]}$ = –6 to +3) isotope compositions (Sack et al., 2020; Colpron et al., 2022). Late Triassic to Early Jurassic plutons that intrude Stikinia and Yukon-Tanana west of the Whitehorse trough show a progressive trend toward more-evolved isotopic values, or an isotopic pull-down, with time (Colpron et al., 2022). The $^{40}Ar/^{39}Ar$ mica cooling dates from the Aishihik batholith (Fig. 2; Long Lake suite) are consistent with exhumation rates of 0.5–2.8 mm/yr (Clark, 2017; Sack et al., 2020).

East of the Big Salmon–Teslin fault system, mafic to felsic plutons of the Lokken suite (Sinemurian to Pliensbachian, 195–184 Ma) that intrude the Yukon-Tanana terrane (Fig. 2) represent the northern extension of Quesnellia arc magmatism in Yukon. Lokken suite plutons have metaluminous geochemical signatures and whole-rock $\varepsilon Nd_{(t)}$ values of –4.3 to –0.6 and zircon $\varepsilon Hf_{(t)}$ values of –2.9 to +9.3 (Sack et al., 2020; Colpron et al., 2022). The Lokken suite plutons were emplaced at relatively shallow crustal depths (~3 kbar) and cooled rapidly (≤2 m.y.) compared to plutons west of the Whitehorse trough. Plutons of the Early Jurassic Minto, Long Lake, and Lokken suites contain inherited Late Triassic–Early Jurassic, Permian, Mississippian, Devonian, and Precambrian zircon cores derived from local Intermontane terrane country rocks (Colpron et al., 2022).

Posttectonic plutons of the Bryde and Fourth of July suites (Aalenian to Bajocian, 174–168 Ma) intruded Stikinia, the Cache Creek terrane, and overlapping strata of the Whitehorse trough after their imbrication in the Middle Jurassic (Fig. 2; Mihalynuk et al., 2004; Sack et al., 2020). These intrusive units have mafic to felsic alkaline compositions and generally yield whole-rock Nd ($\varepsilon Nd_{[t]}$ = +0.5 to +3.5) and zircon Hf (mostly $\varepsilon Hf_{[t]}$ = +4 to +8) isotope values that show a return to juvenile or superchondritic compositions. This ca. 174 Ma isotopic shift was coincident with the end of marine deposition in the Whitehorse trough and beginning of surface uplift recorded by overlying Upper Jurassic to Lower Cretaceous terrestrial strata of the Tantalus Formation, which filled confined intermontane valleys (Long, 2015). Colpron et al. (2022) suggested that the combined evidence for surface uplift and rapid shift to juvenile isotopic compositions reflects lithospheric delamination after imbrication of the Intermontane terranes.

LABERGE GROUP STRATIGRAPHY

The Whitehorse trough extends >600 km from Carmacks in central Yukon to Dease Lake in northern British Columbia (Fig. 1). Lower to Middle Jurassic rocks of the Tanglefoot and Richthofen formations (Laberge Group) define the Whitehorse trough in Yukon and comprise ~3000 m of siliciclastic strata that unconformably overlie the Stikinia and Cache Creek terranes (Figs. 2 and 3; Wheeler, 1961; Tempelman-Kluit, 1984, 2009; Dickie and Hein, 1995; Lowey, 2008; Colpron et al., 2015). The Whitehorse trough was deformed by southwest-verging folds and thrust faults during the Late Jurassic and Cretaceous, most likely in association with dextral transpression along the Teslin-Braeburn fault system (White et al., 2012).

The Tanglefoot formation consists of sandstone, mudstone, and conglomerate units with coal, terrestrial plant material, and vertebrate fossils that are indicative of marginal-marine environments, whereas the Richthofen formation contains graded siltstone to sandstone and mudstone couplets and conglomerate units with ammonites, belemnites, planktonic fossils, and trace fossils (*Helminthopsis*, *Phycosiphon*, *Planolites*) characteristic of deep-marine environments (Wheeler, 1961; Tempelman-Kluit, 1984, 2009; Long, 1986; Hart, 1997; Lowey, 2004; van Drecht et al., 2017; van Drecht and Beranek, 2018). Tanglefoot and Richthofen formation strata are restricted to the northern and central regions of the Whitehorse trough, respectively, suggesting a south-directed deepening of the basin (Fig. 2; Tempelman-Kluit, 1984, 2009; Dickie and Hein, 1995; Lowey, 2004, 2008; Hutchison, 2017). Felsic tuff and epiclastic rock units assigned to the Nordenskiöld member occur in both formations (Figs. 2 and 3) and record Pliensbachian (188–186 Ma) eruptive events coeval with intrusions of the Long Lake suite to the west (Colpron and Friedman, 2008).

Clast- to matrix-supported, polymictic, cobble to boulder conglomerate units occur in the Tanglefoot and Richthofen formations and represent debris-flow, sheetflood, and bar deposits of a fan-delta system (Dickie and Hein, 1995; Hart et al., 1995; Lowey, 2004; van Drecht et al., 2017). Paleoflow indicators suggest fan lobe migration and predominately show east- to northeast- and southwest-directed sediment transport along the western and eastern edges of the Whitehorse trough, respectively. Sediment pathways for the conglomerate units were typically transverse to the longitudinal axis of the Whitehorse trough (e.g., Wheeler, 1961; Dickie and Hein, 1995; Hart et al., 1995; Lowey, 2004). In northern British Columbia, Inklin Formation strata (equivalent to the Richthofen formation) show that longitudinal (north-directed) Sinemurian paleoflow was replaced by transverse Pliensbachian paleoflow (Johannson et al., 1997). Conglomerate clast types include augite-phyric basalt, andesite, tuff, granite, granodiorite, diorite, sandstone, volcanogenic sandstone, and limestone (Hart et al., 1995). Basal conglomerate units are dominated by volcanic and sedimentary clasts, whereas younger strata contain a larger proportion of plutonic clasts, which imply unroofing of the adjacent arc (Dickie and Hein, 1995; Hart et al., 1995; Johannson et al., 1997; Shirmohammad et al., 2011). Pliensbachian–Toarcian conglomerate units in northern British Columbia locally contain eclogite clasts that indicate rapid Early Jurassic exhumation at rates of ~4.1 mm/yr (Canil et al., 2006; Kellett et al., 2018). U-Pb dates of plutonic clasts and detrital zircon grains from the Laberge Group have yielded Late Triassic to Early Jurassic and minor Paleozoic age populations that indicate sources from local Intermontane terrane basement and collision-related plutons (Hart et al., 1995; Gordey et al., 1998; Colpron et al., 2015; Kellett and Iraheta Muniz, 2019; Kellett and Zagorevski, 2021).

MATERIALS AND METHODS

Twelve rock samples were analyzed for detrital zircon U-Pb geochronology and Hf isotope geochemistry at Memorial University of Newfoundland (Table 1; Fig. 2). Laboratory analyses were conducted using the laser-ablation split-stream technique using two inductively coupled plasma–mass spectrometers (e.g., Fisher et al., 2014). Laser-ablation techniques and data reduction protocols are outlined in the Appendix. Detrital zircon U-Pb-Hf isotope results and reference material values are reported in the Supplemental Material (Table S1[1]). U-Pb dates are presented in probability density plots (PDPs) made with a Microsoft Excel macro developed at the Arizona LaserChron Center (https://sites.google.com/a/laserchron.org/laserchron/). Initial $^{176}Hf/^{177}Hf$ ratios are reported as $\varepsilon Hf_{(t)}$ and represent isotopic compositions at the time of crystallization relative to the chondritic uniform reservoir (CHUR). The $\varepsilon Hf_{(t)}$ versus U-Pb age plots show the depleted mantle array (Vervoort and Blichert-Toft, 1999) and crustal evolution lines that use $^{176}Lu/^{177}Hf = 0.015$ (Goodge and Vervoort, 2006). Statistical comparisons (cross-correlation, likeness, and similarity coefficients of PDPs, Kolmogorov-Smirnov and Kuiper tests) were conducted with the DZstats MATLAB program of Saylor and Sundell (2016), and results are reported in the Supplemental Material (Table S2). We followed the statistical assessments of Saylor and Sundell (2016) and favor cross-correlation coefficients (R^2 values range from 0 to 1, with a cross-plot value of 1 indicating identical age peaks) for interpretation purposes because they are sensitive to the presence or absence, relative magnitude, and shape of age peaks in PDPs. Multidimensional scaling (MDS) plots were constructed with the DZmds MATLAB program of Saylor et al. (2018) to compare U-Pb age results with potential sources and stratigraphic correlations.

The youngest detrital zircon crystals in each sample were used to estimate the maximum depositional ages of Laberge Group strata. Three techniques were used: (1) the youngest statistical peak (YSP) method, which takes a weighted mean of the youngest population of two or more grains that yield

[1]Supplemental Material. Table S1: Detrital zircon U-Pb-Hf isotope results and reference material values at Memorial University of Newfoundland. Table S2: Statistical assessments of Laberge Group strata. Table S3: Fossil compilation for Laberge Group strata. Please visit **https://doi.org/10.1130/GEOS.S.20128379** to access the supplemental material, and contact editing@geosociety.org with any questions.

TABLE 1. LOCATION, SUMMARY INFORMATION, AND MAXIMUM DEPOSITIONAL AGE ESTIMATES FOR LABERGE GROUP STRATA

Number on figures	Field sample name	Latitude (°N)	Longitude (°W)	Reference	Comments	CA-TIMS	± (Ma)	YSP (Ma)	± (Ma)	MSWD	YSC (Ma)	± (Ma)	YPP (Ma)	MDA range
Tanglefoot formation														
T1	Eagles Nest	62.0237	135.8226	Colpron et al. (2015)	Basal unit along Robert Campbell Highway; overlies Upper Triassic limestone	–	–	197.8	1.1	1.0	189.9	3.3	200	Hettangian–Pliensbachian
T2	16-LVD-001C	62.0272	135.8492	This study	Basal unit along Robert Campbell Highway; overlies Upper Triassic limestone	–	–	196.7	1.0	1.2	191.0	1.2	200	Hettangian–Sinemurian
T3	16-LVD-001B	62.0272	135.8492	This study	Sandstone along Robert Campbell Highway above basal unit	–	–	188.0	0.4	1.0	185.9	0.4	195	Sinemurian–Pliensbachian
T4	17-LVD-018	61.6286	135.8690	This study	Conglomerate Mountain exposures along Klondike Highway	–	–	184.9	0.9	2.3	187.2	0.7	187	Pliensbachian
T5	16-LVD-004	62.1220	136.2174	This study	Sandstone along Robert Campbell Highway that regionally overlies 187 Ma tuff	–	–	183.6	0.5	1.0	176.0	0.8	185	Pliensbachian–Toarcian
T6	04MC002	62.1117	136.1490	Colpron et al. (2015)	Sandstone along Robert Campbell Highway near Tantalus Butte	–	–	180.4	2.1	1.0	179.6	2.3	195	Pliensbachian–Toarcian
Richthofen formation														
R1	11MC183	60.1837	134.6850	Colpron et al. (2015)	Sandstone along Tagish Road near Carcross	–	–	208.7	1.2	1.0	201.6	2.6	212	Norian–Hettangian
R2	16EB-257-1	61.1909	135.1328	Bordet et al. (2019)	Basal unit along eastern side of Lake Laberge; overlies Upper Triassic limestone	203.46	0.14	203.6	1.1	1.0	195.3	3.8	206	Rhaetian–Sinemurian
R3	15EB-304	61.1042	134.7580	Bordet et al. (2019)	Basal unit along eastern side of Lake Laberge; overlies Upper Triassic limestone	–	–	202.6	1.5	1.0	199.1	2.0	202	Rhaetian–Sinemurian
R4	16EB-394	61.2503	135.1888	Bordet et al. (2019)	Sandstone along eastern side of Lake Laberge	199.78	0.06	196.9	1.5	1.0	192.2	2.3	200	Hettangian–Sinemurian
R5	16-LVD-009	61.0270	134.8620	This study	Basal unit on Mount Laurier; overlies Upper Triassic limestone	–	–	197.7	0.7	1.1	194.5	0.8	205	Rhaetian–Sinemurian
R6	16-LVD-021	61.1109	135.1619	This study	Matrix from polymictic conglomerate on Richthofen Island, Lake Laberge	–	–	197.5	1.1	1.5	195.0	1.1	210	Norian–Sinemurian
R7	12LB220	60.5082	134.1221	Colpron et al. (2015)	Sandstone east of Marsh Lake	–	–	197.2	1.7	1.0	191.5	2.6	198	Sinemurian–Pliensbachian
R8	16-LVD-022	61.1383	135.1188	This study	Sandstone along eastern side of Lake Laberge	–	–	194.9	0.9	1.1	194.9	0.9	205	Rhaetian–Sinemurian
R9	17-LVD-027	60.8746	135.2194	This study	Basal unit north of Takhini River; overlies Upper Triassic limestone	–	–	193.7	0.6	0.9	191.4	0.7	198	Sinemurian–Pliensbachian
R10	16-LVD-023	61.1016	135.0830	This study	Sandstone along eastern side of Lake Laberge	–	–	191.9	2.3	1.0	185.1	1.0	185	Sinemurian–Pliensbachian
R11	04SJP603	61.0760	135.1965	Colpron et al. (2015)	Richthofen formation type area along western side of Lake Laberge	–	–	190.9	0.8	1.3	189.1	1.2	198	Sinemurian–Pliensbachian
R12	17-LVD-030	60.9546	134.2698	This study	Basal unit on Mount Byng; overlies Upper Triassic limestone	–	–	186.5	0.7	1.3	184.0	0.7	176	Pliensbachian–Toarcian
R13	16EB-181	61.0994	135.0577	Bordet et al. (2019)	Sandstone along eastern side of Lake Laberge	186.22	0.09	186.0	1.2	1.1	184.1	1.5	197	Sinemurian–Toarcian
R14	16EB-384	61.2106	135.0755	Bordet et al. (2019)	Sandstone along eastern side of Lake Laberge	186.38	0.07	185.7	1.8	1.0	183.7	2.3	198	Sinemurian–Toarcian
R15	08MC091	60.6653	134.9095	Colpron et al. (2015)	Basal unit on Grey Mountain; overlies Upper Triassic limestone	–	–	181.9	2.6	1.1	177.3	4.5	200	Hettangian–Aalenian
R16	17-LVD-034	60.8998	134.7332	This study	Basal unit on Mount Slim; overlies Upper Triassic limestone	–	–	184.1	1.6	1.4	184.3	1.1	185	Pliensbachian–Toarcian
R17	04SJP594	60.8527	135.4326	Colpron et al. (2015)	Matrix from polymictic conglomerate to the west of Whitehorse	–	–	180.6	1.5	1.6	180.3	1.2	188	Pliensbachian–Toarcian
R18	GL04180b	60.6997	135.3736	Colpron et al. (2015)	Basal unit in Whitehorse area; overlies Upper Triassic tuff and limestone	–	–	179.1	1.3	1.0	178.4	1.5	186	Pliensbachian–Toarcian
R19	17-LVD-038	60.8176	135.4711	This study	Basal unit northwest of Whitehorse; overlies Late Triassic (216 Ma) gabbro	–	–	173.7	0.8	1.1	174.5	1.0	173	Toarcian–Aalenian

Note: Bold indicates sample was collected from basal strata of the Laberge Group. En dash indicates that there are no data for the sample. CA-TIMS—chemical abrasion–thermal ionization mass spectrometry, MDA—maximum depositional age, MSWD—mean square of weighted deviates, YPP—youngest graphical peak method, YSC–youngest cluster at 2σ method, YSP—youngest statistical peak method.

a mean square of weighted deviates (MSWD) ≈ 1 (Coutts et al., 2019; Herriott et al., 2019); (2) the youngest cluster at two sigma (YSC) method, which takes the weighted mean of the youngest three or more grains that overlap at 2σ (Dickinson and Gehrels, 2009); and (3) the youngest graphical peak (YPP) method, which is calculated by the youngest peak age in a probability density plot (Dickinson and Gehrels, 2009), in this case determined by the AgePick Excel macro program developed at the Arizona LaserChron Center.

RESULTS

Tanglefoot Formation

Buff-green, cross-bedded feldspathic lithic arenite that overlies Aksala formation limestone (<20 m above contact) is the stratigraphically lowest part of the Tanglefoot formation sampled along the Robert Campbell Highway, ~25 km east of Carmacks (sample T2 in Fig. 4; Table 1). The sample mostly yielded 252–191 Ma (98%) detrital zircon grains with age peaks of 201 Ma and 228 Ma (Fig. 5A). Detrital zircon grains that ranged 213–191 Ma and 242–217 Ma gave $\varepsilon Hf_{(t)}$ values that clustered between –0.2 to +5 and +10 to +12, respectively (Fig. 5C). A Pennsylvanian zircon grain (308 ± 3 Ma) yielded an $\varepsilon Hf_{(t)}$ value of +2.4.

Buff-colored, medium- to very coarse-grained, feldspathic lithic arenite was collected 15 m above sample T2 along the Robert Campbell Highway (sample T3 in Fig. 4; Table 1), and it gave a 219–185 Ma population with an age peak of 195 Ma (Fig. 5B). The Late Triassic to Early Jurassic population had $\varepsilon Hf_{(t)}$ values that ranged from –4.7 to +9.4 with a dominant cluster between –4.7 and –2.6 (Fig. 5C). Two Mississippian zircon grains of 342 ± 7 Ma and 353 ± 11 Ma had $\varepsilon Hf_{(t)}$ values of –3.8 and +4.1, respectively.

Maroon, medium- to coarse-grained, feldspathic lithic arenite that crops out at Conglomerate Mountain, along the Klondike Highway ~40 km south of Carmacks (sample T4 in Fig. 2; Table 1), yielded a bimodal distribution of Late Triassic to Early Jurassic (48%) and Late Devonian to Early Triassic (52%) zircon grains (Fig. 5D). The 221–180 Ma population yielded age peaks of 187 Ma and 205 Ma and $\varepsilon Hf_{(t)}$ values of +0.9 to +11.5 (Fig. 5F). Late Devonian to Early Triassic zircon grains produced a 313 Ma age peak and $\varepsilon Hf_{(t)}$ values that ranged from +5.7 to +12.7.

A sample of buff-colored lithic arenite was collected from the stratigraphically highest Tanglefoot formation near Tantalus Butte along the Robert Campbell Highway (sample T5 in Fig. 4; Table 1). Tanglefoot strata in this area are overlain by Upper Jurassic to Lower Cretaceous conglomerate of the Tantalus Formation and are projected to overlie a Pliensbachian crystal lithic tuff horizon to the east (187.1 ± 0.2 Ma; Colpron and Friedman, 2008). This sample mostly contained 212–176 Ma (92%) detrital zircon grains with an age peak of 185 Ma (Fig. 5E). Most $\varepsilon Hf_{(t)}$ values of Late Triassic to Early Jurassic grains ranged from –4.3 to +4.8, and one 212 Ma zircon yielded a $\varepsilon Hf_{(t)}$ value of +8.8 (Fig. 5F). An early to mid-Paleozoic (8%) population yielded an age peak of 338 Ma and $\varepsilon Hf_{(t)}$ values between –8.7 and –5.7. Two Middle Mississippian zircon grains had $\varepsilon Hf_{(t)}$ values of +4 and +8.7.

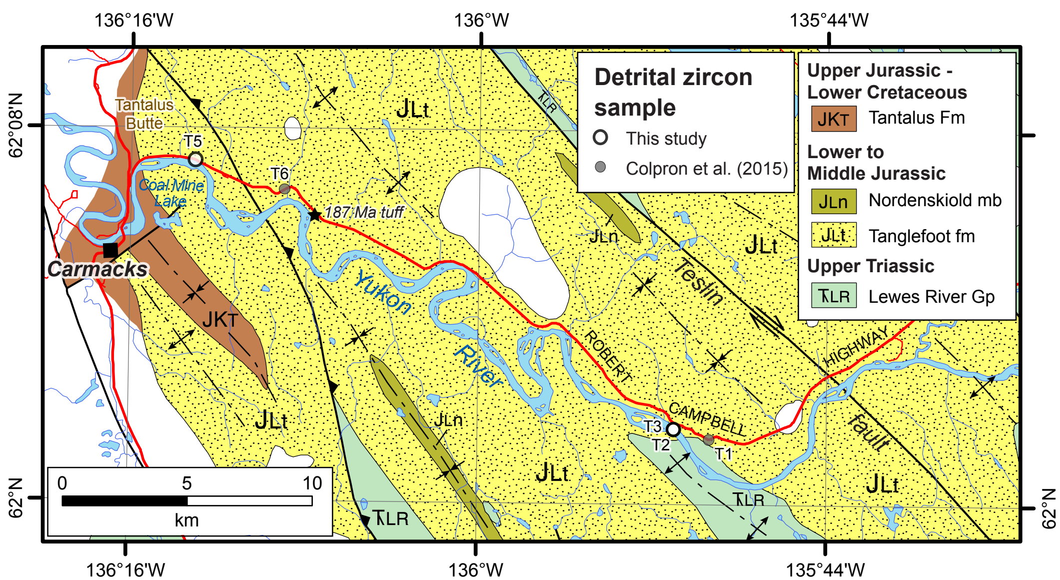

Figure 4. Geology of the northern Whitehorse trough near Carmacks, Yukon, Canada. Locations of detrital zircon samples from the Tanglefoot formation and from a Pliensbachian tuff horizon (ca. 187 Ma; Colpron and Friedman, 2008) are shown. White areas are Cretaceous and younger cover. Abbreviations: fm—formation; mb—member; Gp—Group.

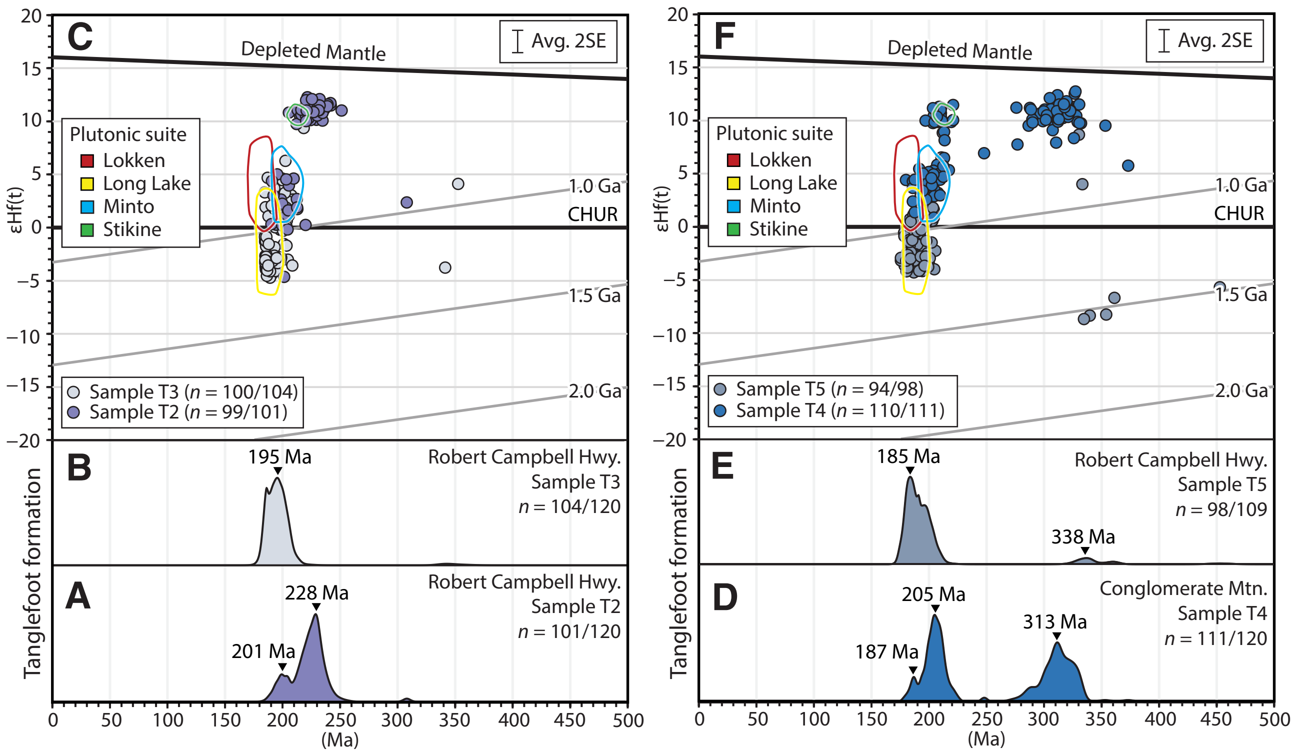

Figure 5. Detrital zircon results for Tanglefoot formation rock units. (A) Robert Campbell Highway (Hwy.) feldspathic lithic arenite (sample T2). (B) Robert Campbell Highway feldspathic lithic arenite (sample T3). (D) Conglomerate Mountain (Mtn.), Klondike Highway feldspathic lithic arenite (sample T4). (E) Robert Campbell Highway lithic arenite (sample T5). (C, F) εHf$_{(t)}$ vs. U-Pb age diagrams for Tanglefoot formation samples. Total number of analyses is presented with the results; for example, *n* = 101/120 indicates that 120 analyses for sample 16-LVD-001C yielded 101 ages that passed the discordance filter and were used for interpretation. The Appendix contains supporting information about the laser-ablation methods used. CHUR—chondritic uniform reservoir; SE—standard error.

Richthofen Formation

Parallel laminated, fine- to medium-grained, feldspathic lithic arenite that disconformably overlies Aksala formation limestone (<5 m above contact) along the eastern flank of Mount Laurier, ~40 km northeast of Whitehorse (sample R5 in Fig. 6; Table 1), yielded 290–225 Ma (58%) detrital zircon grains with an age peak of 205 Ma (Fig. 7A) and εHf$_{(t)}$ values of +3 to +6.3 (Fig. 7I). Mississippian to Permian zircon grains (42%) showed a broad age range from 356 ± 8 Ma to 269 ± 4 Ma with a probability age peak ca. 329 Ma and εHf$_{(t)}$ values of +2.3 to +10.7 (Fig. 7E).

Matrix-supported polymictic conglomerate on Richthofen Island regionally overlies Aksala formation limestone in the Lake Laberge area, ~40 km north of Whitehorse (sample R6 in Fig. 6; Table 1). A sample of green feldspathic lithic arenite matrix yielded 232–186 Ma (97%) zircon grains with an age peak of 210 Ma (Fig. 7B). Late Triassic to Early Jurassic zircon grains had εHf$_{(t)}$ values that ranged from +3.1 to +13.9 with a main cluster between +4.4 and +7.8 (Fig. 7E). Three Paleozoic zircon grains of 340 ± 7 Ma, 343 ± 10 Ma, and 464 ± 8 Ma yielded εHf$_{(t)}$ values at +11.8, +12.8, and +8.2, respectively.

Lithic feldspathic arenite in faulted contact with Aksala formation limestone (sample R8 in Fig. 6; Table 1) along the eastern shoreline of Lake Laberge yielded 217–194 Ma (98%) detrital zircon grains with an age peak of 205 Ma (Fig. 7C). Late Triassic to Early Jurassic zircon grains gave εHf$_{(t)}$ values that clustered between +2.8 and +5.3 and one zircon with a εHf$_{(t)}$ value of –0.2 (Fig. 7E). Two Middle Mississippian zircon grains at 333 ± 5 Ma and 339 ± 6 Ma yielded εHf$_{(t)}$ values of +6.3 and +5.4, respectively.

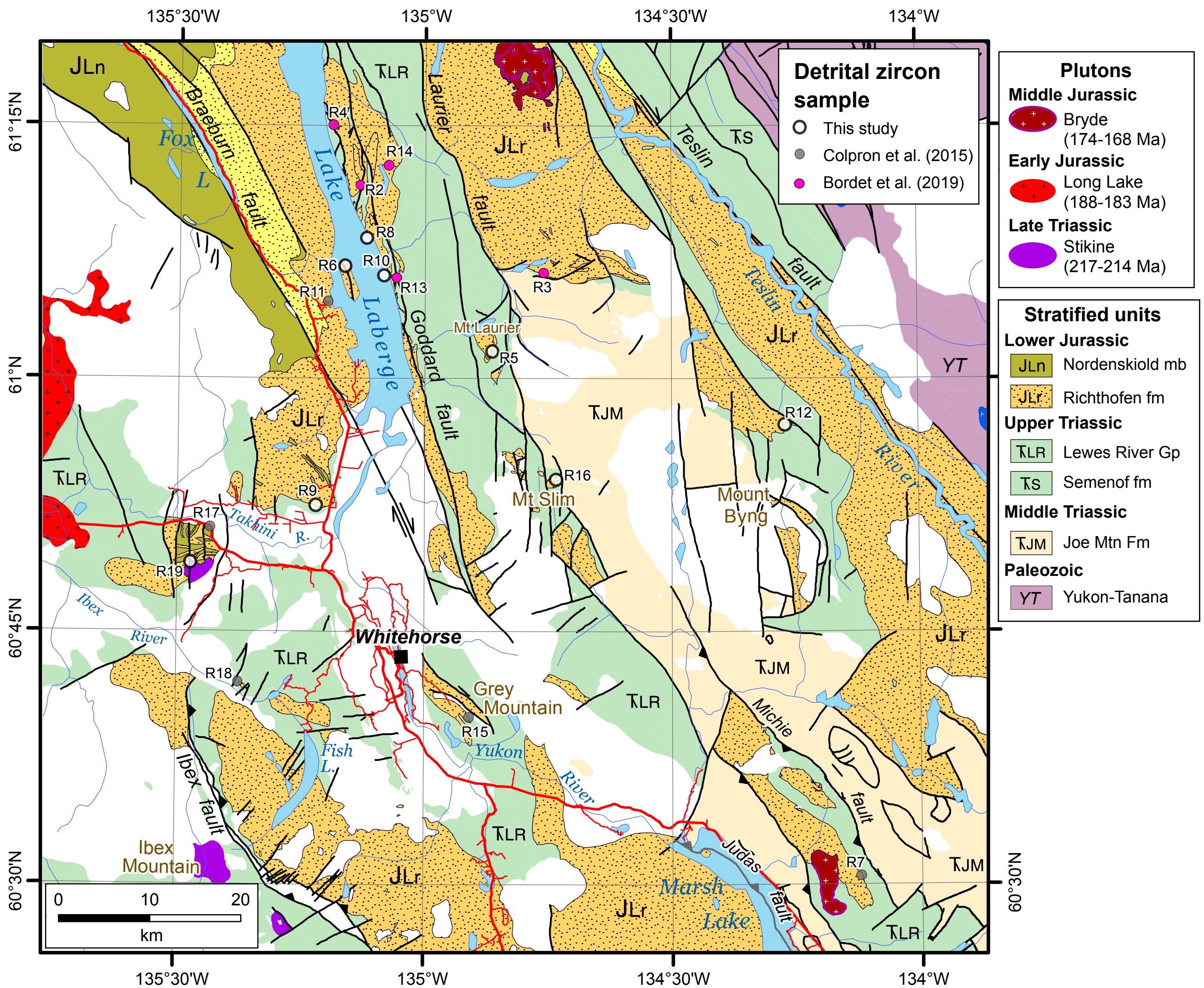

Figure 6. Geology of the Intermontane terranes and Whitehorse trough near Whitehorse, Yukon, Canada. Locations of detrital zircon samples from strata of the Richthofen formation are shown. White areas are Cretaceous and younger cover. Abbreviations: fm—formation; mb—member; Gp—Group; Mtn—Mountain; L.—Lake; R.—River.

Blue-gray, bioclastic lithic wacke that disconformably overlies Aksala formation limestone (<5 m above contact) north of the Takhini River, ~20 km northwest of Whitehorse (sample R9 in Fig. 6; Table 1), contains Lower to Middle Jurassic *Pinna* sp. (bivalve) and undetermined coarse-ribbed pectinoid bivalve and ammonite fossils (R. Blodgett, 2018, personal commun.). This sample yielded 216–181 Ma (96%) detrital zircon grains with an age peak of 198 Ma and $\varepsilon Hf_{(t)}$ values that ranged from +4.9 to +12.1 (Figs. 7D and 7E). Two Pennsylvanian grains at 315 ± 9 Ma and 359 ± 6 Ma were also recognized in this sample.

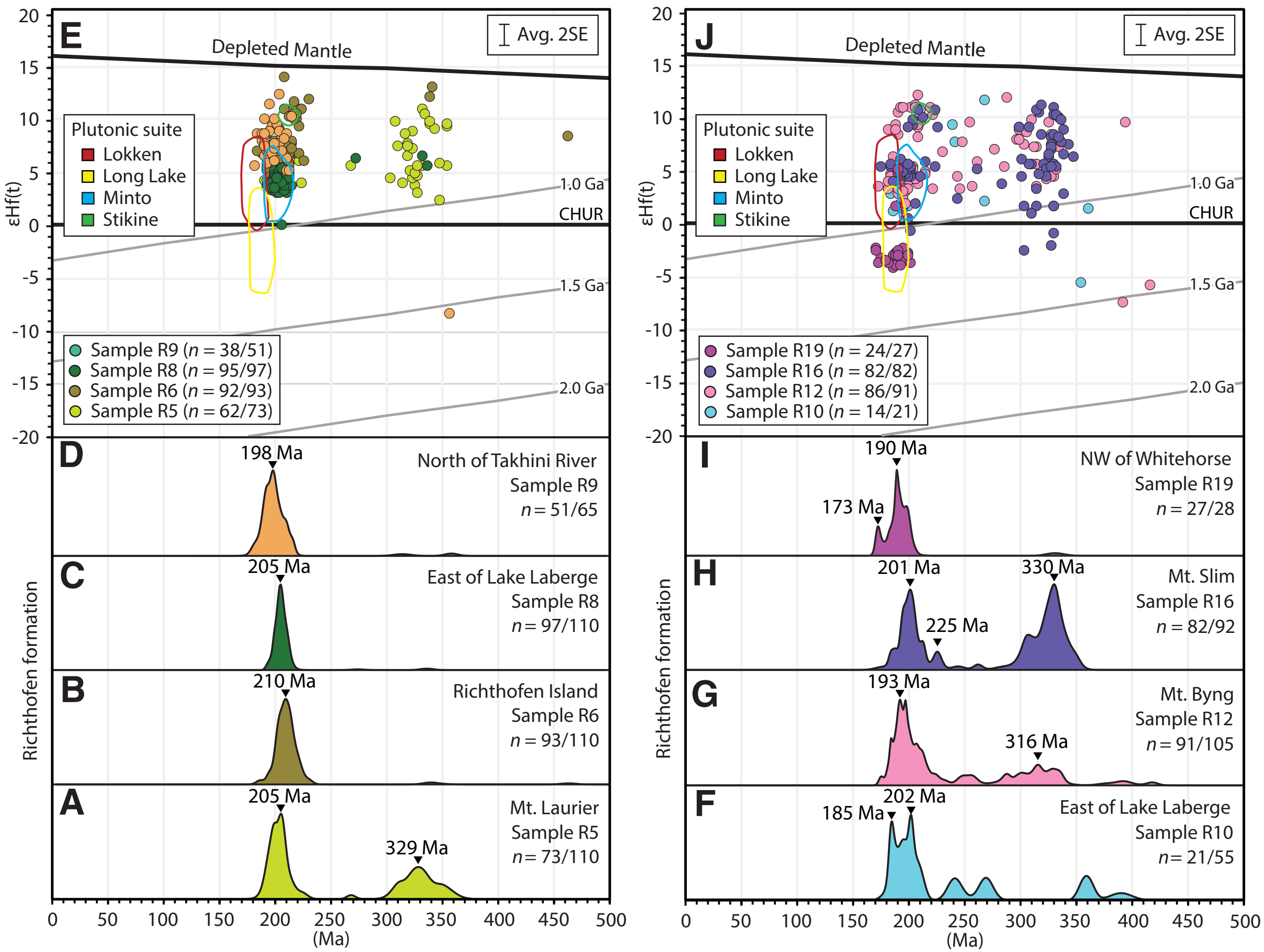

Figure 7. Detrital zircon results for Richthofen formation rock units. (A) Mount Laurier feldspathic lithic arenite (sample R5). (B) Feldspathic lithic arenite matrix from Richthofen Island conglomerate (sample R6). (C) Feldspathic lithic arenite along eastern side of Lake Laberge (sample R8). (D) Takhini subdivision bioclastic lithic wacke (sample R9). (F) Lithic wacke along eastern side of Lake Laberge (sample R10). (G) Mount Byng lithic wacke (sample R12). (H) Mount Slim feldspathic lithic arenite (sample R16). (I) King Lake epiclastic rocks (sample R19). (E, J) $\varepsilon Hf_{(t)}$ vs. U-Pb age diagrams for Richthofen formation samples. CHUR—chondritic uniform reservoir; SE—standard error.

Lithic wacke with mudstone rip-up clasts was collected along the eastern shoreline of Lake Laberge (sample R10 in Fig. 6; Table 1). This sample mostly yielded 270–185 Ma zircon grains (72%) with age peaks of 185 and 202 Ma (Fig. 7F). Late Triassic to Early Jurassic zircon grains had $\varepsilon Hf_{(t)}$ values between +0.9 and +2.6 (Fig. 7J). Mid-Permian to Middle Triassic zircon grains at 270 ± 8 Ma, 269 ± 6 Ma, 244 ± 8 Ma, and 244 ± 6 Ma gave $\varepsilon Hf_{(t)}$ values of −3.9, +5.6, +3.9, and +2.2, respectively. Three Middle Devonian to Early Mississippian (14%) zircon grains yielded 356 ± 4 Ma ($\varepsilon Hf_{(t)}$ = −5.8), 363 ± 6 Ma ($\varepsilon Hf_{(t)}$ = +1.2), and 390 ± 10 Ma ages. Three Precambrian (14%) zircon grains were also present at 1474 ± 51 Ma, 2563 ± 26 Ma ($\varepsilon Hf_{(t)}$ = +0.9), and 2829 ± 23 Ma.

Dark gray-blue, medium-grained, lithic wacke that overlies pebble to cobble limestone conglomerate and Aksala formation limestone (<10 m above contact) near Mount Byng, ~50 km northeast of Whitehorse (sample R12 in Fig. 6; Table 1), yielded 250–175 Ma (67%) detrital zircon grains with an age peak of 193 Ma (Fig. 7G). Late Triassic to Early Jurassic zircon grains gave $\varepsilon Hf_{(t)}$ values between +1.7 and +12 with two clusters around +4 and +10 (Fig. 7J). Silurian to Permian detrital zircon grains (33%) made up a broad population that ranged from 419 to 257 Ma and yielded age peaks of 251, 254, 289, 301, 316, 328, and 392 Ma (Fig. 7G). Silurian to Permian zircon grains gave $\varepsilon Hf_{(t)}$ values between –7.6 and +11.8.

Dark-gray to buff, fine- to medium-grained, feldspathic lithic arenite that overlies Aksala formation limestone at Mount Slim (<10 m above contact), ~30 km northeast of Whitehorse (sample R16 in Fig. 6; Table 1), contained 244–178 Ma detrital zircon grains with age peaks of 225, 201, and 185 Ma (Fig. 7H). Mississippian to Permian (59%) zircon grains ranged from 350 ± 4 Ma to 262 ± 5 Ma with probability age peaks at ca. 330 and 310 Ma (Fig. 7H). Middle Triassic to Early Jurassic zircon grains yielded $\varepsilon Hf_{(t)}$ values of –3.2 to +10.6, and Paleozoic zircon grains gave values that ranged from –2.7 to +10.9 (Fig. 7J). One Paleoproterozoic zircon at 2263 ± 74 Ma yielded a $\varepsilon Hf_{(t)}$ value of –10.8.

Epiclastic rocks nonconformably overlie 216 Ma gabbro of the Stikine suite (Sack et al., 2020) south of the Alaska Highway, ~20 km northwest of Whitehorse (sample R19 in Fig. 6; Table 1). This basal sample (<1 m above contact) was dominantly composed of 203–172 Ma (96%) detrital zircon grains with age peaks at 190 Ma and 173 Ma (Fig. 7I). Late Triassic to Middle Jurassic detrital zircon grains gave $\varepsilon Hf_{(t)}$ values that ranged from –4.1 to +5 (Fig. 7J).

MAXIMUM DEPOSITIONAL AGE ESTIMATIONS

Tanglefoot formation strata yielded Hettangian to Toarcian maximum depositional ages (Table 1) that are consistent with Early to Middle Jurassic benthic macrofossils in the Laberge Group (Table S3, see footnote 1; e.g., Colpron et al., 2007b; Lowey, 2008; Colpron, 2011). Using the YSC and YSP methods, the latter of which was shown by Herriott et al. (2019) to correlate best with corresponding chemical abrasion–isotope dilution thermal ionization mass spectrometry (CA-TIMS) analyses, new (this study) and published (recalculated from Colpron et al., 2015) samples of the basal Tanglefoot formation confirm that subsidence in the northern reaches of the Whitehorse trough began by the Sinemurian (Table 1). Tanglefoot formation strata above the basal Sinemurian succession consistently yielded Pliensbachian depositional ages using the YSP method (Table 1). In the case of sample T3, the YSP estimated age (188.0 ± 0.4 Ma) is most consistent with a stratigraphic position below a Pliensbachian tuff (187.1 ± 0.2 Ma; Colpron and Friedman, 2008) ~17 km to the west along the Robert Campbell Highway (Fig. 4), whereas the YSC estimation (185.9 ± 0.3 Ma) would suggest a position above the dated tuff horizon.

Richthofen formation strata overlie the Upper Triassic Lewes River Group and older rocks at several locations in central Yukon (Lowey, 2008; Colpron et al., 2015). Nineteen new (this study) and published (recalculated from Colpron et al., 2015; Bordet et al., 2019) samples, including nine basal sandstones that overlie Lewes River Group rocks, yielded Late Triassic to Middle Jurassic maximum depositional ages for the Richthofen formation (Table 1). The maximum depositional ages for five of the samples reported in Bordet et al. (2019) were determined using CA-TIMS methods and agree with the YSP estimates in four of our samples (Table 1). The other sample (R4) has a CA-TIMS date that most closely matches the YPP estimate of the maximum depositional age. Three samples with Late Triassic YSP estimates reported in Colpron et al. (2015) and Bordet et al. (2019) have maximum depositional ages that are older than biostratigraphic constraints for the Laberge Group, which suggests recycling of underlying Norian to Rhaetian rocks of the Lewes River Group. Most (11 of 19) Richthofen formation samples have Sinemurian to Pliensbachian age estimates and confirm coeval deposition with Tanglefoot formation units farther north. Four basal sandstone units, including epiclastic rocks west of Whitehorse that sit nonconformably on 216 Ma gabbro, yielded Toarcian to Aalenian YSP estimates, which show that subsidence along the west flank of the Whitehorse trough continued into the Middle Jurassic.

DETRITAL ZIRCON PROVENANCE INTERPRETATIONS

Mesozoic Age Populations

Triassic to Jurassic detrital zircon grains (40%–99% of each sample, $\bar{X}$ = 79%) are interpreted to have provenance from arc and collision-related Mesozoic igneous rocks. Primary sources include mafic to felsic intrusive suites (and eroded volcanic equivalents) in southern Yukon that are well characterized by zircon CA-TIMS U-Pb, zircon Hf isotope, and whole-rock Nd-Sr-Pb isotope geochemical studies (Sack et al., 2020). For example, Sinemurian to Pliensbachian strata of the Tanglefoot formation along the Robert Campbell Highway (samples T2 and T3) contain Late Triassic to Early Jurassic zircon grains with chondritic to superchondritic Hf isotope compositions (Fig. 5) that are consistent with provenance from ca. 205–194 Ma Minto suite plutons near the northern apex of the Whitehorse trough (Fig. 2; Colpron et al., 2022). A Pliensbachian sandstone along the Robert Campbell Highway (sample T5) has subchondritic Early Jurassic zircon grains consistent with provenance from ca. 188–183 Ma Long Lake suite rocks to the west of the Whitehorse trough, which show a range of $\varepsilon Hf_{(t)}$ values from +6.4 to –5.8 (Sack et al., 2020; Colpron et al., 2022).

Richthofen formation strata contain Triassic to Early Jurassic detrital zircon grains with dominantly chondritic to superchondritic Hf isotope compositions (Fig. 7) that are consistent with provenance from ca. 217–214 Ma Stikine and ca. 205–194 Ma Minto intrusive suite rocks (Sack et al., 2020). Samples with significant late Sinemurian and younger (≤195 Ma) detrital zircon populations also generally have chondritic to superchondritic Hf isotope compositions that may indicate sources in the ca. 195–184 Ma Lokken suite to the east, which typically has more juvenile $\varepsilon Hf_{(t)}$ values compared to coeval intrusions of the

Long Lake suite (Colpron et al., 2022). An exception is sample R19, an epiclastic unit with a Toarcian to Aalenian maximum depositional age that sits nonconformably on 216 Ma gabbro west of Whitehorse, in which late Sinemurian and younger detrital zircons have subchondritic $\varepsilon Hf_{(t)}$ values, which are more common in plutons of the Long Lake suite to the west.

Paleozoic Age Populations

Paleozoic detrital zircon grains (<1%–59% of each sample, $\bar{X}$ = 19%) are interpreted to have provenance from Devonian to Permian igneous rocks of the Yukon-Tanana and Stikinia terranes that form the basement to Late Triassic arc assemblages and host Late Triassic to Early Jurassic intrusive suites in southern Yukon. Late Devonian to Mississippian detrital zircon grains, such as those at Conglomerate Mountain (sample T5; Fig. 2) and east of Lake Laberge (sample R10; Fig. 6), show subchondritic Hf isotope compositions (Fig. 7) that are consistent with primary and recycled sources in the Yukon-Tanana terrane (Finlayson assemblage and related intrusive suites; Murphy et al., 2006; Piercey et al., 2006). Superchondritic Late Mississippian to Pennsylvanian detrital zircon grains in the Tanglefoot formation (Conglomerate Mountain) and Richthofen formation (Mount Laurier, Mount Slim, Mount Byng; Fig. 6) yielded ca. 315 Ma and 330 Ma peaks and suggest sources in the Takhini and Boswell assemblages of Stikinia that crop out along the flanks of the Whitehorse trough (Fig. 2; Hart, 1997; Simard et al., 2003; Bordet et al., 2019).

Precambrian Age Populations

Precambrian detrital zircon grains were observed in only two samples of the Richthofen formation (R10 and R16). They are interpreted to be recycled from local exposures of pre–Late Devonian metasedimentary successions in the Yukon-Tanana terrane (Snowcap assemblage; Piercey and Colpron, 2009).

DISCUSSION

Whitehorse Trough Subsidence and Filling Patterns

The Whitehorse trough has been interpreted as a forearc basin that developed in proximity to the Stikinia arc as a result of subduction of the Cache Creek ocean (part of Panthalassa; Mihalynuk et al., 1994; Dickie and Hein, 1995; English and Johnston, 2005). Colpron et al. (2015) showed that deposition of the Laberge Group was coincident with rapid exhumation of metamorphic rocks and their contained intrusions along the flanks of the trough. They suggested that the Whitehorse trough first developed as a forearc basin that evolved into a syncollisional, piggyback basin in the Early Jurassic during early growth of the northern Cordilleran orogen. Our new U-Pb-Hf isotope data and maximum depositional age calculations for Laberge Group strata, in combination with improved constraints on the magmatic and metamorphic evolution of the Intermontane terranes (Clark, 2017; Sack et al., 2020; Gaidies et al., 2021; Colpron et al., 2022), provide new opportunities to evaluate the filling patterns of the Whitehorse trough.

Figure 8 shows the maximum depositional age estimations of Laberge Group strata for two broad transects along and across the Whitehorse trough in southern Yukon. Nineteen samples of the Richthofen formation, including the YSP ages of nine basal sandstones (Table 1), illustrate that submarine fan and fan-delta deposits record subsidence events that likely correspond to late Rhaetian to early Sinemurian, late Sinemurian to Pliensbachian, and Toarcian regional exhumation. Six samples of Tanglefoot formation strata, including the YSP ages of two basal sandstones (Fig. 8; Table 1), also indicate that the oldest marginal-marine deposits in the northern Whitehorse trough could be linked to early Sinemurian exhumation. Colpron et al. (2015) noted, based on a limited number of samples (n = 8) and using YPP estimates, that maximum depositional ages from basal strata (n = 4) appear to be progressively younger toward the west. They suggested that an early uplift event along the western side of the Whitehorse trough was followed by western transgression of Laberge Group strata during the Sinemurian to Toarcian. To test this hypothesis and better resolve initial subsidence within the trough, half of the new samples reported in this study (n = 6/12) were collected from basal strata of the Laberge Group. Our analysis of maximum depositional ages, using a larger number of samples (n = 25; Table 1) and YSP estimates, confirms that the youngest basal Laberge strata (Toarcian–Aalenian) that sit unconformably on Lewes River Group rocks occur mostly along the western edge of Whitehorse trough exposures, but this data set also illustrates a more complex age pattern near the center of the trough (Fig. 8).

Pliensbachian to Toarcian basal strata of the Richthofen formation that cover Upper Triassic reefal limestone at Grey Mountain (sample R15) and Mount Slim (R16), east of Whitehorse (Fig. 6), have maximum depositional ages that are considerably younger than basal and nonbasal strata to the north, near Lake Laberge (Fig. 8). This suggests that reef complexes of the Aksala formation in the Whitehorse area remained as topographic highs for most of the Early Jurassic or that tectonic exhumation processes in the central Whitehorse trough were focused on the Grey Mountain and Mount Slim region during the Pliensbachian–Toarcian.

Richthofen formation strata collected near Mount Byng (sample R12) along the eastern edge of the trough have Pliensbachian to Toarcian maximum depositional ages (Figs. 6 and 8; Table 1) and suggest that the flanks of the Whitehorse trough were highlands early in basin development, perhaps associated with basin-bounding faults, and they only subsided in the Pliensbachian–Toarcian. The pattern of maximum depositional ages along strike of the trough shows generally younger estimated ages in shallow-marine strata of the Tanglefoot formation in the north, and mostly older estimated ages in more distal strata of the Richthofen formation near Lake Laberge, to the south (Fig. 8).

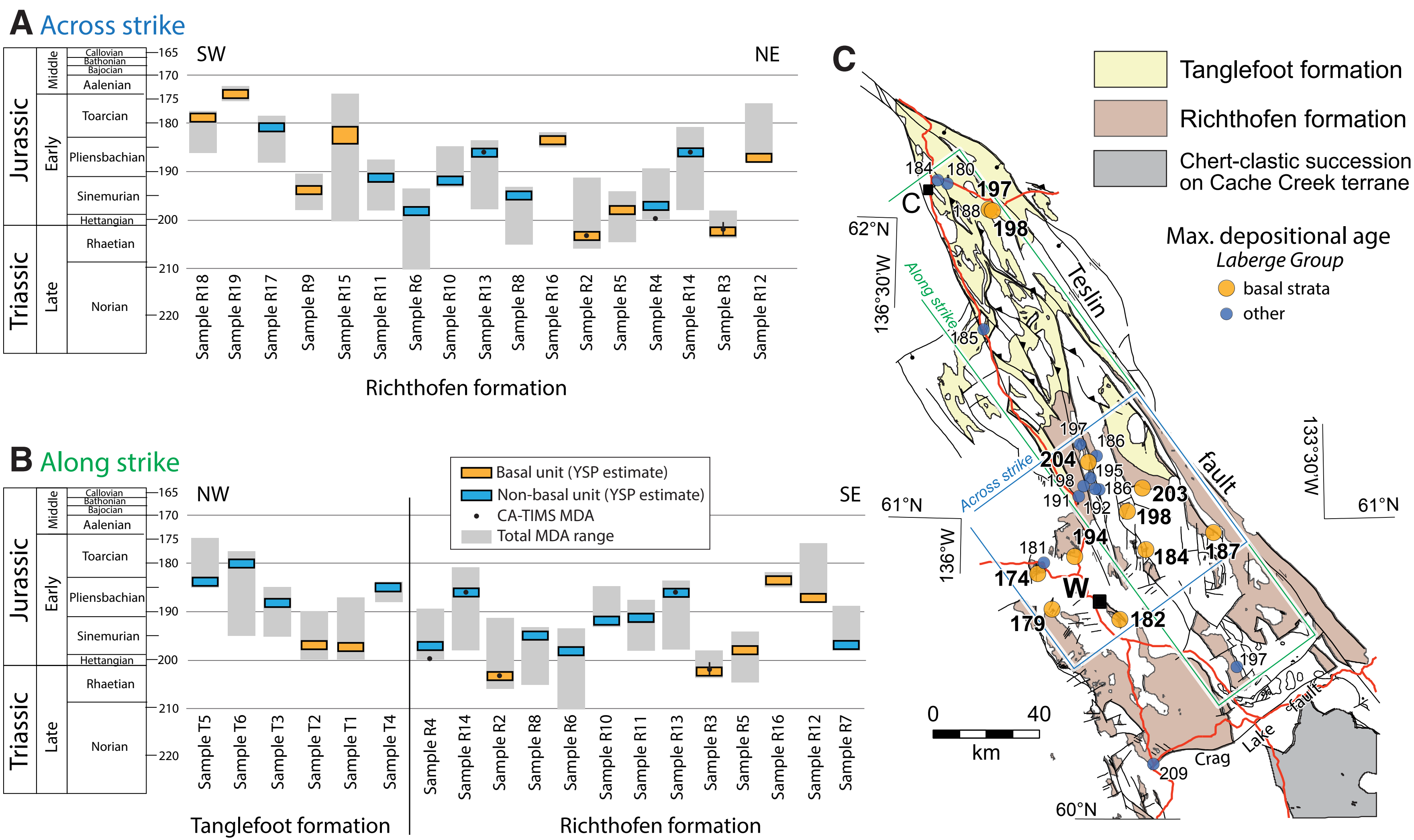

Figure 8. Graphs of Laberge Group maximum depositional ages for two broad transects (A) across and (B) along strike of the Whitehorse trough. Basal and nonbasal strata are shown by orange and blue boxes, respectively, using the youngest statistical peak (YSP) metric of Coutts et al. (2019). Gray boxes show total maximum depositional age (MDA) range for each sample reported in Table 1. (C) Map showing distribution of Laberge Group sedimentary units and samples collected from basal (orange) and nonbasal (blue) strata. Maximum depositional ages are labeled with those from basal strata shown in bold. C—Carmacks; W—Whitehorse; CA-TIMS—chemical abrasion–thermal ionization mass spectrometry.

Jurassic Tectonic Evolution and Development of the Whitehorse Trough

Colpron et al. (2015) proposed that crustal thickening and exhumation of the Yukon-Tanana terrane in Yukon mark the onset of early Mesozoic orogenic activity in the northern Cordillera. In their model, the northern Intermontane terranes and Whitehorse trough were part of the growing orogen that advanced onto western North America during the Early to Middle Jurassic and formed part of the hinterland-retroarc thrust belt system that supplied sediment to the oldest foreland basin successions of western Canada (Poulton, 1989). Colpron et al. (2015) framed the Late Triassic to Jurassic evolution of the northern Cordillera in the context of the oroclinal enclosure model of Mihalynuk et al. (1994). New evidence regarding the metamorphic history of the Yukon-Tanana terrane (Clark, 2017; Dyer, 2020; Gaidies et al., 2021), documentation of syncollisional, Early Jurassic plutons in southern Yukon (Sack et al., 2020; Colpron et al., 2022), and the development of the latest Triassic to Early Jurassic Hazelton arc in British Columbia (George et al., 2021; Nelson et al., 2022) have led to revised models in which end-on collision of the Stikinia arc with the Yukon-Tanana and Quesnellia terranes in the latest Triassic to Early Jurassic initiated the development of the northern Cordilleran orogen. Colpron et al. (2022) provided a model that proposes the collision zone in Yukon was linked by a sinistral transform fault system to the retreating Hazelton arc to the south (Nelson et al., 2022). Detrital zircon U-Pb-Hf isotope results from synorogenic strata of the Laberge Group (Table 1) combined with statistical assessments (Fig. 9; Table S2, see footnote 1), biostratigraphic constraints (Table S3; Colpron, 2011), and published tuff ages (Colpron and Friedman, 2008) provide the opportunity to reevaluate the position of the Whitehorse trough in this revised Late Triassic to Jurassic tectonic framework for the northern Cordilleran orogen.

Figure 10 shows a series of maps that illustrate filling patterns and progressive development of the Whitehorse trough during the Early to Middle Jurassic. These maps were constructed using the present distribution of Laberge Group strata in Yukon and depositional age constraints in Table 1 and Table S3. The present structural geometry of the Whitehorse trough is the result of Cretaceous (and younger?) dextral transpression superposed on older Jurassic structures (Colpron, 2011; White et al., 2012; Calvert et al., 2017). Fold and thrust structures in the northern Whitehorse trough are gentle and suggest shortening on the order of 15%–30% (White et al., 2012). However, the amount of transcurrent displacement along intrabasin faults is largely unconstrained, and a rigorous palinspastic restoration of the Whitehorse trough region was not attempted for these maps. Nevertheless, the older histories of some intrabasin faults (e.g., Laurier, Goddard, and Braeburn faults) can still be inferred based on truncation of stratigraphic trends (dashed red lines in Fig. 10; Colpron et al., 2007b; White et al., 2012) and facies changes (Bordet et al., 2019). Figure 11 is a schematic representation of the tectonic evolution of sedimentary basins in the northern Intermontane terranes following the model of Colpron et al. (2022).

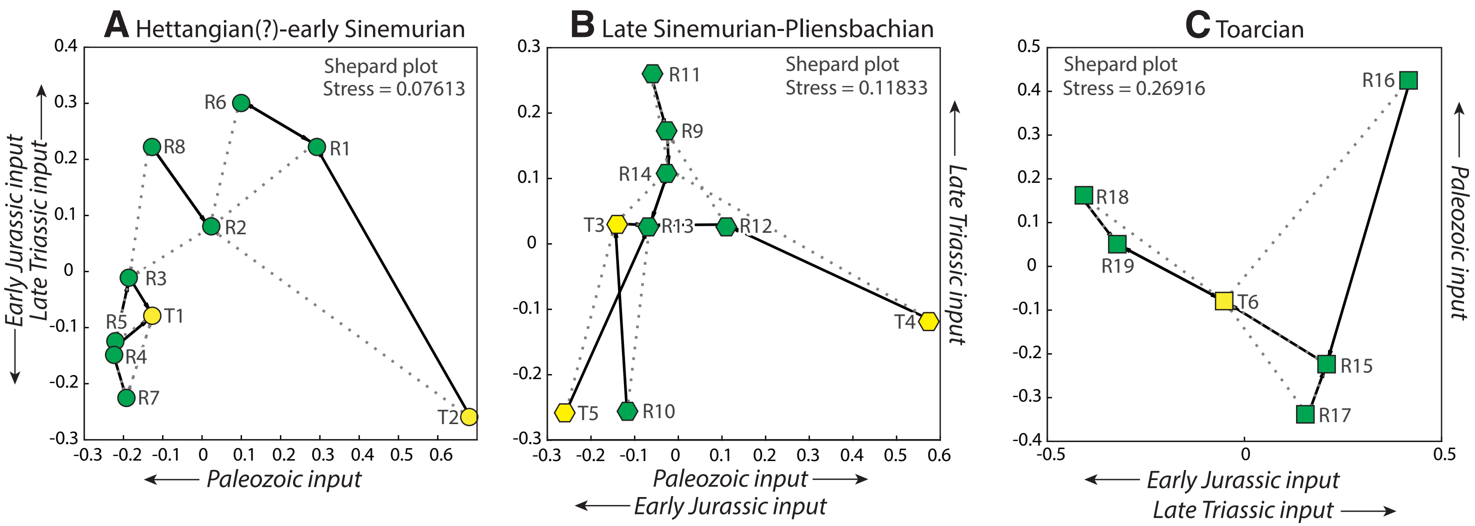

Figure 9. Multidimensional scaling plots of Laberge Group detrital zircon U-Pb age distributions. (A) Hettangian(?)–early Sinemurian strata. (B) Late Sinemurian–Pliensbachian strata. (C) Toarcian strata. The plots were generated with the DZmds routine of Saylor et al. (2018) and used the cross-correlation coefficient to calculate dissimilarity. Corresponding Shepard plots are available in Table S2 (see text footnote 1).

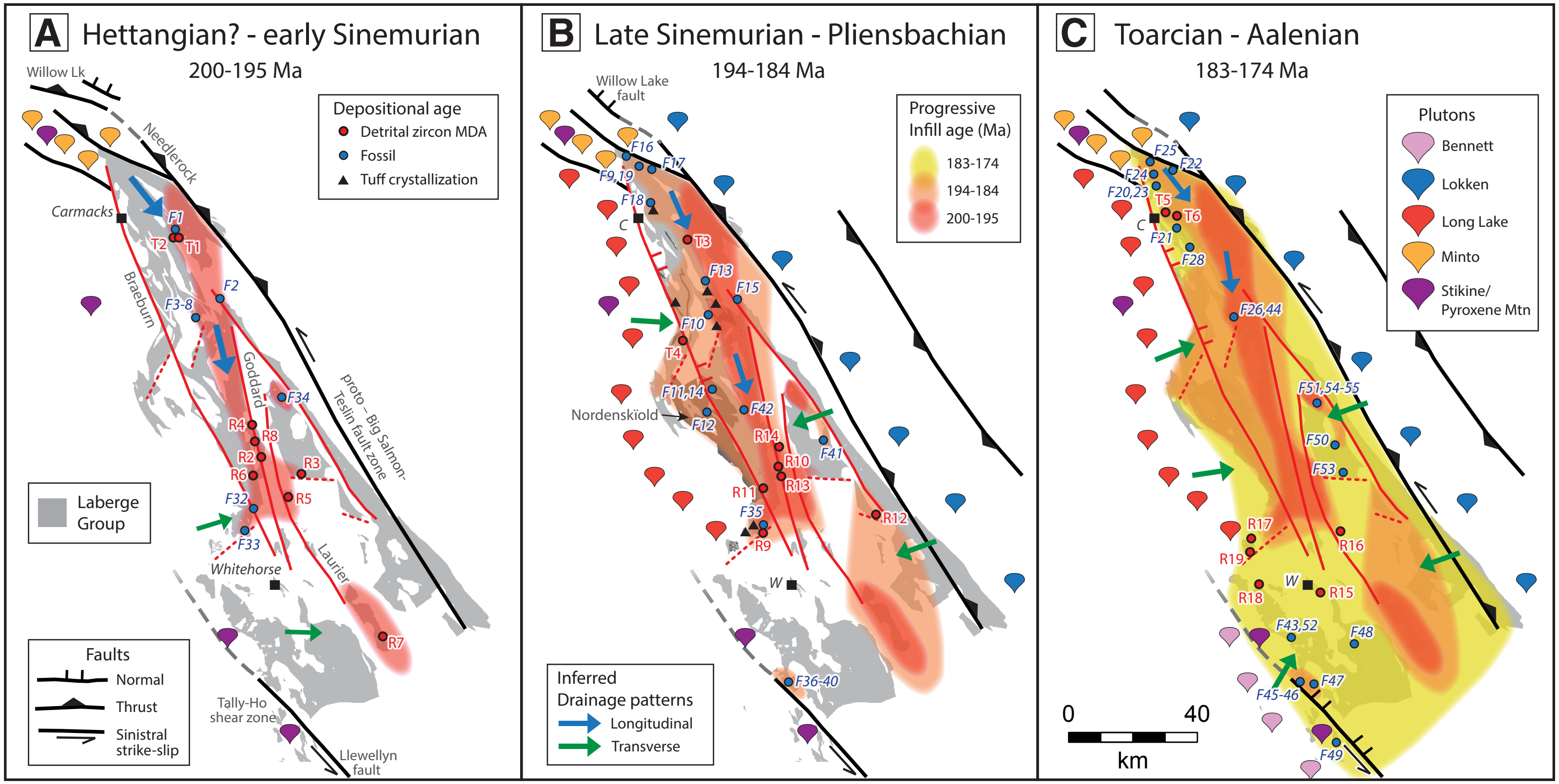

Figure 10. Jurassic subsidence and infill patterns for the Whitehorse trough in southern Yukon. (A) Hettangian(?)–early Sinemurian. (B) Late Sinemurian–Pliensbachian. (C) Toarcian–Aalenian. Detrital zircon maximum depositional ages (MDAs) are from Table 1. Selected fossil collections are summarized in Table S3 (see text footnote 1). Tuff crystallization ages are from Colpron and Friedman (2008). Blue and green arrows are inferred longitudinal and transverse drainage patterns, respectively, based on Laberge Group detrital zircon results. Solid red lines indicate intrabasin faults inferred to have been active during Whitehorse trough deposition. Faults without ornamentation have unknown sense of displacement. Dashed grey lines are inferred faults. Dashed red lines indicate mapped stratigraphic trends and facies changes within Whitehorse trough. Lk—Lake; Mtn—Mountain.

Hettangian(?) to Early Sinemurian

The latest Triassic to earliest Jurassic end-on collision of Stikinia (Fig. 11A) was probably triggered by the northwest advance of North America as Pangea began to breakup (Monger and Gibson, 2019; George et al., 2021; Colpron et al., 2015, 2022). Collision-related processes are documented by Early Jurassic tectonic burial and amphibolite-facies metamorphism in the Yukon-Tanana terrane (Johnston et al., 1996; Berman et al., 2007; Clark, 2017; Gaidies et al., 2021). The peraluminous, syncollisional 205–194 Ma plutons of the Minto suite were emplaced at midcrustal depths during deformation (Sack et al., 2020; Colpron et al., 2022); deposition of Laberge Group strata in the Whitehorse trough also began at that time (Figs. 10A and 11B; Colpron et al., 2015).

Crustal thickening was followed by exhumation of the Yukon-Tanana terrane (Figs. 11B and 11C) and its contained syncollisional plutons beginning in the Sinemurian (Clark, 2017; Colpron et al., 2022). The Willow Lake fault (Fig. 2; Colpron and Ryan, 2010) is a northwest-striking extensional fault that provides evidence for crustal-scale, Early Jurassic tectonic exhumation of the Yukon-Tanana terrane during the initial deposition of Laberge Group

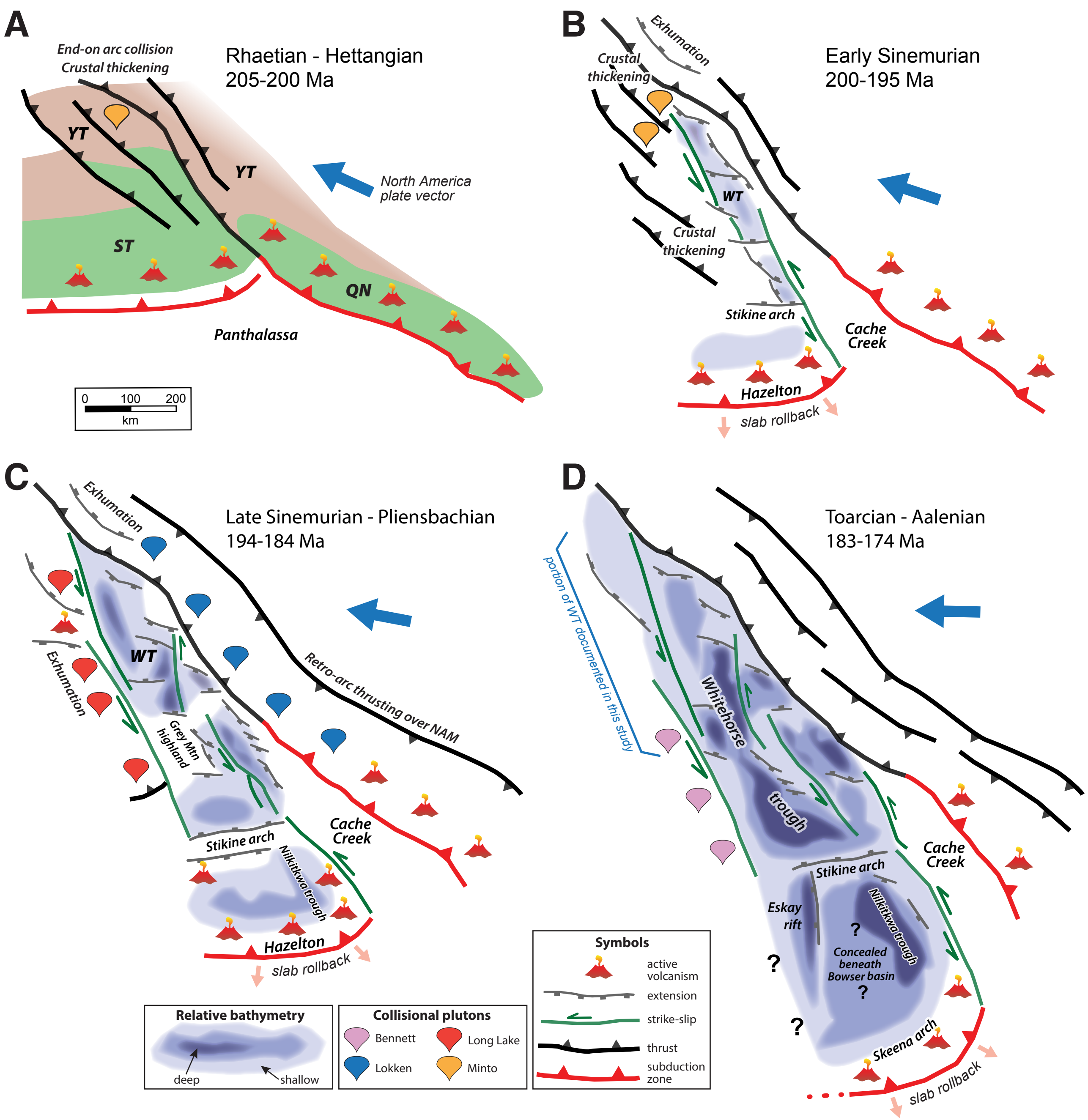

Figure 11. Schematic tectonic model for development of Early to Middle Jurassic sedimentary basins in the northern Intermontane terranes (modeled after George et al., 2021; Nelson et al., 2022; Colpron et al., 2022). Schematic palinspastic maps highlight mainly the evolution of the Whitehorse trough and Hazelton arc of Stikinia. The Whitehorse trough (WT) was probably connected to Early Jurassic forearc strata in the Cache Creek terrane (Colpron et al., 2015), but relative bathymetry in the Cache Creek is not illustrated here. (A) End-on arc collision of Stikinia (ST) and Yukon-Tanana (YT)/Quesnellia (QN) in the latest Triassic initiated crustal thickening in the northern Cordillera. (B) In the early Sinemurian, as collision progressed in the north, the Hazelton arc retreated to the south, and initial subsidence of the Whitehorse trough occurred in a narrow, transtensional axial basin north of the Stikine arch. Plutons of the Minto suite were intruded in the collision zone. (C) By the late Sinemurian to Pliensbachian, more widespread subsidence occurred in most of Whitehorse trough, but local highlands remained (e.g., Grey Mountain area). South of the Stikine arch, subsidence occurred in the Hazelton trough behind the retreating arc (Gagnon et al., 2009; Nelson et al., 2022). (D) By the Toarcian, subsidence reached its maximum extent in the Whitehorse trough, and the upper Hazelton Group onlapped the Stikine arch. To the south, the Eskay rift was developed in the Aalenian. NAM—North America.

strata. The hanging wall of the Willow Lake fault consists of undeformed and unmetamorphosed rocks with Mississippian cooling ages (Knight et al., 2013). Polydeformed metamorphic rocks in the footwall of the Willow Lake fault yield ca. 197 Ma and younger $^{40}Ar/^{39}Ar$ biotite and hornblende ages, which, in combination with 205–196 Ma cooling ages for Rhaetian plutons of the region, support rapid Early Jurassic exhumation of basement and collision-related plutons from midcrustal depths (Berman et al., 2007; Knight et al., 2013). For example, early Sinemurian rocks of the Tatchun batholith (Fig. 2) that occur on the northeastern flank of the Whitehorse trough were exhumed during the Early Jurassic at 2.1–7.5 mm/yr (Sack et al., 2020).

Sinemurian subsidence in the Whitehorse trough in Yukon was probably facilitated by sinistral transtension as a transform fault system developed together with the reorganization of subduction after collision (Figs. 10A and 11B; Colpron et al., 2022). The depositional life span (<20 m.y.) and sediment accumulation rates (>0.2 mm/yr, decompacted) recorded by Laberge Group strata support the initiation of the Whitehorse trough as a strike-slip basin fed by drainage systems along rapidly exhuming flanks. In their study of Laberge Group strata in Yukon, Dickie and Hein (1995) proposed that Lower to Middle Jurassic submarine fan deposits are consistent with rapid tectonic subsidence adjacent to basin-bounding, strike-slip faults. Potential candidates for the western boundaries of the Whitehorse trough include the Tally Ho and Llewellyn fault zones near the Yukon–British Columbia border (Fig. 2) where early ductile fabrics are inferred to have developed during Late Triassic to Early Jurassic sinistral strike-slip displacement (Hart and Radloff, 1990; Currie and Parrish, 1993; Mihalynuk et al., 1999). The proto–Big Salmon–Teslin fault system was the eastern boundary of the Whitehorse trough (Colpron et al., 2022) and accommodated early sinistral displacement (de Keijzer et al., 2000). Potential intrabasin faults that may have been involved in the development of the Whitehorse trough include the Braeburn, Goddard, and Laurier faults, which locally bound distinct pre-Jurassic domains (Colpron et al., 2007b; White et al., 2012; Bordet et al., 2019). For example, the Laurier fault juxtaposes different Triassic successions (Joe Mountain formation on the east, Lewes River Group on the west) and is overlapped by Norian to Rhaetian Aksala formation rocks (Fig. 6; Bordet et al., 2019). The oldest maximum depositional age estimates and fossil determinations for Laberge Group strata (Fig. 6; samples R1 to R8 in Fig. 10A) occur mainly in the axial regions of the Whitehorse trough, especially near Lake Laberge, in proximity to the Goddard and Laurier faults.

Early Sinemurian terrestrial to marginal-marine strata of the Tanglefoot formation (samples T1 and T2 in Fig. 10A) yielded 201 Ma age peaks and indicate that Minto suite sources, including the rapidly exhumed Granite Mountain and Tatchun plutons, fed sediment routing systems near the northern apex of the Whitehorse trough. A population of Ladinian to Norian (ca. 242–230 Ma) detrital zircon grains with superchondritic Hf isotope compositions in sample T2 further suggests that point sources in the Joe Mountain and Povoas formations were locally sampled in the Carmacks area. To the south, early Sinemurian submarine fan deposits of the Richthofen formation (e.g., samples R4 to R8 in Fig. 10A) yielded unimodal 210–200 Ma age peaks that are consistent with Minto suite sources to the northwest of the Whitehorse trough. North-to-south, early Sinemurian stratigraphic connections are undetermined in the Whitehorse trough, but sample T1 notably yielded PDP cross-correlation coefficients of 0.71–0.98 ($\bar{X}$ = 0.88) and 0.66–0.95 ($\bar{X}$ = 0.70) when compared with Richthofen formation samples R1–R4 (from Colpron et al., 2015; Bordet et al., 2019) and R5–R8 (this study), respectively. Based on the number of grains analyzed (see Saylor and Sundell, 2016), we do not reject the hypothesis that these early Sinemurian or older strata were drawn from the same sources. The MDS plot in Figure 9A further shows that early Sinemurian Tanglefoot formation strata cluster or have similarity with some of the oldest Richthofen formation samples (R3–R5, R7), which further suggests common provenance areas during that time. Most of these Richthofen formation strata crop out around the southern Braeburn, Goddard, and Laurier faults, and these structures may have controlled north-to-south axial drainage patterns (Fig. 10A). Sample T2 is a statistical outlier because of its unique 242–230 Ma population, and it is distanced from Richthofen formation samples in the MDS plot, which implies dissimilarity, but its nearest neighbor (black tie line) is sample R1 (Fig. 9A). Late Devonian to Late Pennsylvanian (360–300 Ma; 329 Ma peak; Fig. 7A) detrital zircon grains in the basal sandstone at Mount Laurier (sample R5 in Fig. 10A) are consistent with Yukon-Tanana provenance (Klinkit assemblage, Piercey et al., 2006), but may also point to contributions from the age-equivalent Boswell and Takhini assemblages of Stikinia near the northeastern and western basin flanks, respectively (Hart, 1997; Colpron, 2011; Bordet et al., 2019; Fig. 2). The detrital zircon U-Pb-Hf isotope results for these Tanglefoot and Richthofen formation strata are interpreted to support the early Sinemurian establishment of longitudinal drainage along the axis of the Whitehorse trough.

Late Sinemurian to Pliensbachian

Southward migration of the Hazelton arc in the Early Jurassic (Fig. 11B; Nelson et al., 2022) led to continued development of a sinistral transform system that progressively enclosed the northern Cache Creek terrane (Colpron et al., 2022). Sinistral transtension in Yukon promoted continued exhumation of the flanks of the Whitehorse trough and plutons of the Long Lake and Lokken suites that had been intruded at mid- to upper-crustal levels to the west and east of Whitehorse trough, respectively (Fig. 2; Sack et al., 2020). Laberge Group strata accordingly documented subsidence resulting from late Sinemurian to Pliensbachian tectonic exhumation processes and were mostly deposited in the northwestern sector of the basin (Figs. 10B and 11C).

Late Sinemurian to Pliensbachian strata in the Carmacks area yielded 205–185 Ma age peaks from Minto and Long Lake suite sources and generally showed lower $\varepsilon Hf_{(t)}$ values than those recognized in older strata. For example, early Sinemurian sandstone along the Robert Campbell Highway has Late Triassic to Early Jurassic detrital zircon grains with $\varepsilon Hf_{(t)}$ values that generally range from 0 to +5, whereas overlying late Sinemurian to Pliensbachian strata (samples T3 and T5 in Fig. 10B) have similar-aged grains with $\varepsilon Hf_{(t)}$ values of

–5 to +5 (Figs. 5C and 5F). These excursions toward subchondritic Hf isotope compositions reflect increasing crustal contributions to Long Lake suite magmatism (Sack et al., 2020; Colpron et al., 2022).

Pliensbachian strata at Conglomerate Mountain in the northern Whitehorse trough (sample T4 in Fig. 10B) crop out near the trace of the Braeburn fault, which may have been part of a western bounding fault system that accommodated the exhumation of Triassic–Jurassic and Carboniferous rock units. Conglomerate Mountain strata have age peaks that correspond to Long Lake suite (187 Ma), Minto suite (205 Ma), and Takhini assemblage (313 Ma) sources from the western flank of the Whitehorse trough (Fig. 5D). Late Sinemurian to Pliensbachian strata of the Richthofen formation along the Braeburn and Goddard faults to the south, such as samples R9 to R14 (Fig. 10B), yield PDP cross-correlation coefficients of 0.32–0.54 ($\overline{X}$ = 0.40) when compared to Conglomerate Mountain strata, from which we cannot rule out different or similar sources (e.g., Saylor and Sundell, 2016), but these samples do not cluster together in the MDS plots (Fig. 9B). On the other hand, samples R9 to R14 have detrital zircon U-Pb signatures that are like Pliensbachian samples T3 (PDP cross-correlation coefficients of 0.82–0.94, $\overline{X}$ = 0.89) and T5 (PDP cross-correlation coefficients of 0.54–0.80, $\overline{X}$ = 0.66) along the Robert Campbell Highway, and these cluster together in the MDS plots (Fig. 9B), which is consistent with longitudinal drainage patterns. The detrital zircon Hf isotope compositions of these Richthofen formation rocks, however, do not show the same subchondritic trends as samples T3 and T5 in the northern Whitehorse trough. For example, basal sandstone units that sit on Lewes River Group strata north of the Takhini River and at Mount Byng (samples R9 and R12 in Fig. 10B) have detrital zircon Hf isotope compositions pointing to age-equivalent, but probably different juvenile sources. Sample R9 on the western flank has superchondritic zircon Hf isotope compositions consistent with sources from the Minto suite (Figs. 7D and 7E), perhaps calling for south-directed drainage along the Braeburn fault system, whereas sample R12 on the east flank has zircon Hf isotope compositions that likely indicate sources in the Lokken suite and Yukon-Tanana terrane to the east (Figs. 7G and 7J). These results taken together support late Sinemurian to Pliensbachian establishment of transverse drainage systems in at least some parts of the Whitehorse trough, including near Conglomerate Mountain in the north and near Mount Byng in the south.

Toarcian to Aalenian

Late Early to Middle Jurassic entrapment of the Cache Creek terrane and imbrication of the Intermontane terranes in the northern Canadian Cordillera (Mihalynuk et al., 2004) probably resulted from continued westward drift of North America as the central Atlantic Ocean began to open (Monger and Gibson, 2019; Colpron et al., 2022). Laberge Group strata that coincided with the emplacement of Bennett suite plutons (Figs. 10C and 11D), prior to thrust imbrication of the Stikinia and Cache Creek terranes, are widespread and indicate subsidence from the basin flanks to central axis during the final stages of Whitehorse trough development. At Grey Mountain near Whitehorse, basal Richthofen formation strata (R15 in Fig. 10C) are probably early Toarcian and sit unconformably on Lewes River Group reefal limestone. These Norian to Rhaetian rocks likely formed block-faulted highlands early in the development of the Whitehorse trough, perhaps inherited from a preexisting Triassic fault system along the central axis or a pop-up block within a sinistral strike-slip system, and only subsided during the late Early Jurassic. Other Tanglefoot and Richthofen formation strata (samples T6 and R16–R19), including a Toarcian basal sandstone unit at Mount Slim along the southern Laurier fault, have Late Triassic to Early Jurassic and Paleozoic age populations that may indicate local provenance rather than well-mixed, longitudinal drainage signatures. Statistical comparisons between samples T6 and R15–R19 yielded PDP cross-correlation coefficients of 0.33–0.85 ($\overline{X}$ = 0.65), from which we cannot rule out different or similar sources (e.g., Saylor and Sundell, 2016), but the Richthofen formation samples do show sample T6 as a common neighbor in a MDS plot (Fig. 9C). Basal Richthofen formation strata west of Whitehorse nonconformably overlie Stikine suite gabbro (sample R19 in Fig. 10C) and imply that fault-related highlands along the western flank of the Whitehorse trough did not subside until the Toarcian to Aalenian. This hypothesis can be tested by future investigations of Laberge Group strata in the Fish Lake area to the southwest of Whitehorse (Fig. 6), where there is comparatively less fossil and detrital zircon provenance information.

The northern Intermontane terranes and Laberge Group are intruded by stitching 174–168 Ma plutons of the Bryde suite (Sack et al., 2020) and represent the end of Whitehorse trough deposition. This final phase of Laberge Group deposition is recorded by Aalenian to Bajocian strata that are adjacent to the northern Braeburn fault near Carmacks and the ca. 172 Ma Teslin Crossing pluton near the Teslin fault in the east-central Whitehorse trough (Colpron, 2011; Sack et al., 2020). Upper Jurassic to Lower Cretaceous terrestrial strata of the Tantalus Formation unconformably overlie the Laberge Group marine rocks and document surface uplift associated with lithospheric delamination or slab breakoff after final collision of the northern Intermontane terranes (Colpron et al., 2022).

Implications for Cordilleran Tectonics and Paleogeography

The Triassic to Jurassic tectonic evolution and paleogeography of western North America have long been the subjects of debate, with considerable interest about the timing of Cordilleran terrane accretion and establishment of the hinterland-retroarc thrust belt and foreland basin system (e.g., Murphy et al., 1995; Fuentes et al., 2009; Colpron et al., 2015; LaMaskin et al., 2015; Golding et al., 2016; Beranek et al., 2017; Monger and Gibson, 2019; Pană et al., 2019; Nixon et al., 2020). Crustal thickening and terrane imbrication events in Yukon and British Columbia (e.g., Murphy et al., 1995; Mihalynuk et al., 1999; Nixon et al., 2020) are most consistent with an accreted position for the Intermontane terranes by the Early Jurassic and support the hypothesis that the Whitehorse trough was carried eastward within the nascent Cordilleran orogen (Colpron et al., 2015, 2022). Eastward convergence of the Intermontane terranes with western North America began in the Sinemurian–Pliensbachian (Figs. 10B and 11C; e.g., Nixon et al., 2020). Provenance studies of Fernie Formation strata (see location in Fig. 1), which represent the oldest foreland basin units of western Canada and are coeval with the lower Laberge Group, have recently demonstrated that Sinemurian to Pliensbachian "basal sandstone" rocks yield Late Triassic to Early Jurassic detrital zircon grains (including age peaks of 207 and 192 Ma) sourced from the Intermontane terranes (Pană et al., 2019). Integrated zircon U-Pb and fossil studies have also identified Pliensbachian (188 Ma) bentonitic clay horizons in the lower Fernie Formation and require ash-fall contributions from the Intermontane terranes to the west (Hall et al., 2004), analogous to the ages of the oldest Nordenskiöld member tuffs in the Whitehorse trough (Colpron and Friedman, 2008).

The Early to Middle Jurassic sinistral transform fault system that generated the Whitehorse trough was restricted to the collision zone north of the Stikine arch in the northern Intermontane terranes (Figs. 1 and 11; Colpron et al., 2022; Nelson et al., 2022), but it heralded a profound change in plate dynamics that would later affect outboard regions of the North American Cordillera (Monger and Gibson, 2019). By the late Middle Jurassic, transcurrent regimes accommodated the accretion of the Alexander-Wrangellia-Peninsular composite terrane along the western margins of Stikinia and the Yukon-Tanana terrane (e.g., McClelland and Gehrels, 1990; Gehrels, 2001; McClelland et al., 1992). Middle to Late Jurassic tectonism drove tectonic exhumation and coarse-grained deposition in the Talkeetna forearc and arc regions of southern Alaska (e.g., Trop et al., 2005; Trop and Ridgway, 2007), perhaps along the sinistral Bruin Bay fault system (Betka et al., 2017). The Coast Mountains continental arc system was established along parts of the Insular-Intermontane terrane boundary by the Late Jurassic (van der Heyden, 1992; Gehrels et al., 2009; Beranek et al., 2017). Late Jurassic to Early Cretaceous oblique convergence resulted in a major sinistral transcurrent fault system, which in British Columbia may have accommodated >800 km of displacement, and generation of Oxfordian and younger structural basins at releasing bends, which were in a back-arc position relative to the Coast Mountains arc (e.g., Anderson, 2015).

Implications for the Detrital Zircon Hf Isotope Records of Ancient Orogens

Crustal thickening events can result in lower- to upper-crustal geochemical contributions to arc and collision-related igneous rocks (e.g., Pearce et al., 1984; Ducea et al., 2015). In Andean-type accretionary systems, the underthrusting of melt-fertile lower crust beneath a continental arc during retroarc deformation results in the partial melting of lithosphere with only minor contributions from asthenospheric mantle (Ducea and Barton, 2007; DeCelles et al., 2009). These crustal thickening events are generally identified by upper-plate igneous rocks with subchondritic radiogenic isotope compositions, which contrast with those generated from superchondritic mantle sources during normal, steady-state subduction. It follows that syntectonic siliciclastic strata and their recycled derivatives yield detrital zircon U-Pb ages and Hf isotope compositions capable of constraining increasing crustal contributions to upper-plate magmatic systems (e.g., Laskowski et al., 2013; Pecha et al., 2016; Pepper et al., 2016), including those that transitioned over time from normal, steady-state subduction to arc collision. Late Triassic to Jurassic detrital zircon grains in Laberge Group strata support this hypothesis and generally show increasing crustal contributions or decreasing $\varepsilon Hf_{(t)}$ values with time, replicating the isotopic compositions of their igneous rock sources in the northern Intermontane terranes during the south-progressing collision and entrapment of the Cache Creek terrane (Sack et al., 2020; Colpron et al., 2022). We interpret that 205–194 Ma detrital zircon grains with chondritic to subchondritic Hf isotope compositions in the Tanglefoot formation are the result of latest Triassic to Early Jurassic tectonic burial, prograde metamorphism, and midcrustal emplacement of syncollisional Minto suite plutons.

Stikinia is generally considered to have juvenile basement or to have been constructed from depleted mantle–derived arc rocks with little to no crustal contamination (e.g., Logan et al., 2000; Dostal et al., 2009; Bordet et al., 2019). For example, late Paleozoic detrital zircon grains with Takhini assemblage provenance at Conglomerate Mountain (sample T4) yielded $\varepsilon Hf_{(t)}$ values of +7.8 to +12, which approach the depleted mantle array (Figs. 5D and 5F). However, Colpron et al. (2022) concluded that some Early Jurassic plutons emplaced into northern Stikinia, such as peraluminous Long Lake suite rocks with subchondritic zircon Hf isotope compositions and inherited Paleozoic zircon cores, incorporated old crustal material during arc collision. In northern British Columbia, George et al. (2021) recognized that latest Triassic to Jurassic zircon grains in the Hazelton Group, which were part of the arc system to the south of the active collision zone in Yukon (Figs. 11B–11D), have an average $\varepsilon Hf_{(t)}$ value of +10, but locally these rocks yield early Paleozoic, Proterozoic, and Neoarchean detrital zircon grains derived from basement highs. The crustal affinity or identity of these isotopically evolved materials is uncertain, but the depleted mantle ages of subchondritic Early Jurassic igneous and detrital zircon grains in southern Yukon suggest that Stikinia could have Proterozoic crystalline basement domains or contain sedimentary assemblages that were derived from Precambrian rocks. For example, sample R19 yielded subchondritic 176–172 Ma detrital zircon grains that plot between the 1.0 and 1.5 Ga crustal evolution lines in Figure 7J. A second option for the origin of this crust is that Laurentian cratonal rocks were shoved beneath Stikinia and the Yukon-Tanana terrane as they were carried eastward over the edge of North America during Early Jurassic retroarc thrusting (Fig. 11C). These findings from northern British Columbia and southern Yukon illustrate that high-*n* or targeted detrital zircon U-Pb-Hf isotope studies of arc-proximal basins provide new opportunities to understand the architecture and crustal evolution of Stikinia and, by extension, arc terranes in ancient accretionary and collisional orogens.

CONCLUSIONS

Detrital zircon U-Pb-Hf isotope studies of Laberge Group strata have constrained the timing of syntectonic deposition in the Whitehorse trough and their significance to northern Cordilleran tectonics and paleogeography. Maximum depositional age estimates for Tanglefoot and Richthofen formation strata demonstrate that tectonic subsidence began by the early Sinemurian following latest Triassic–earliest Jurassic end-on arc collision between northern Stikinia and the Yukon-Tanana terrane. The subsequent southward retreat of the Hazelton arc of Stikinia resulted in the development of a sinistral strike-slip fault system that accommodated regional exhumation of the northern Intermontane terranes, syncollisional magmatism, and subsidence of the Whitehorse trough. Early Sinemurian marginal-marine and submarine fan strata have statistically comparable detrital zircon U-Pb-Hf isotope signatures and support the establishment of longitudinal drainage along the axis of the northern Whitehorse trough by ca. 197 Ma. Intrabasin strike-slip faults may have accommodated axial sediment transport from northern source regions near Carmacks to southern depocenters near Whitehorse. Late Sinemurian to Pliensbachian and Toarcian turbidite and debris-fan strata were mostly derived from transverse drainage systems, and they reveal that the flanks of the Whitehorse trough were fault-related highlands that only subsided by the early Middle Jurassic. Early Jurassic detrital zircon grains from the Long Lake plutonic suite show excursions to subchondritic Hf isotope values through time that represent increased crustal contributions to syncollisional magmatism in the collision zone to the north.

APPENDIX

Zircon U-Pb Geochronology and Hf Isotope Geochemistry Methods

Zircon crystals were separated from rock samples, handpicked onto double-sided tape, and mounted in epoxy. After polishing to expose the interior of the crystals, cathodoluminescence imaging of the mounts using a JEOL JSM 7100F scanning electron microscope was completed at the Memorial University of Newfoundland. The images were used to locate homogeneous regions of the zircons and to avoid complex internal structures, cracks, and zones of potential Pb loss.

Isotope ratios were measured using the laser-ablation split-stream method at Memorial University of Newfoundland following the procedures of Hutter and Beranek (2020). Zircon crystals were ablated with a GeoLas 193 nm excimer laser-ablation system using a 40 μm spot size, laser fluence of 5 J/cm^2, pulse rate of 10 Hz, and 600 shots with a total analysis time of ~120 s (~30 s background measurement, ~60 s ablation, and ~30 s washout). Ablated material was evacuated from the ablation chamber via He carrier gas and split using a baffled Y-connector. The Hf isotopes were acquired using a Thermo Finnigan Neptune multicollector–inductively coupled plasma–mass spectrometer (ICP-MS), and U-Pb isotopes were measured using a Thermo Finnigan Element XR magnetic sector ICP-MS. Time-integrated U-Pb signals were analyzed offline using Iolite software (Paton et al., 2010). Age calculations were made using the VizualAge data reduction scheme, which includes a correction routine for down-hole fractionation (Petrus and Kamber, 2012). U-Pb ages were calibrated to the 1065 Ma zircon standard 91500 (Wiedenbeck et al., 1995), and $^{176}Hf/^{177}Hf$ ratios were compared to those of the 337 Ma zircon standard Plešovice (Sláma et al., 2008). Zircon U-Pb analyses with high error (>10% uncertainty) or excessive discordance (>10% discordant, >5% reverse discordant) were excluded from plots and interpretation. The reported ages for grains younger and older than 1200 Ma are based on $^{206}Pb/^{238}U$ and $^{207}Pb/^{206}Pb$ ages, respectively. Age-corrected epsilon Hf ($\varepsilon Hf_{(t)}$) calculations used the decay constant of Söderlund et al. (2004) and present-day chondritic uniform reservoir values of Bouvier et al. (2008).

ACKNOWLEDGMENTS

This project was supported by the Yukon Geological Survey and Natural Sciences and Engineering Research Council of Canada (NSERC) Discovery Grants to Luke Beranek. John Hanchar and Core Research Equipment and Instrument Training (CREAIT) staff members Wanda Aylward, Rebecca Lam, and Markus Wälle aided laboratory studies at Memorial University of Newfoundland. Presubmission feedback on this project from Emily Finzel and Steve Piercey was greatly appreciated. Associate Editor Joel Saylor and journal reviewers Ken Ridgway and Jeff Trop provided constructive and helpful reviews that improved this manuscript. This is Yukon Geological Survey contribution 059.

REFERENCES CITED

Amato, J.M., and Pavlis, T.L., 2010, Detrital zircon ages from the Chugach terrane, southern Alaska, reveal multiple episodes of accretion and erosion in a subduction complex: Geology, v. 38, p. 459–462, https://doi.org/10.1130/G30719.1.

Anderson, T.H., 2015, Jurassic (170–150 Ma) basins: The tracks of a continental-scale fault, the Mexico-Alaska megashear, from the Gulf of Mexico to Alaska, *in* Anderson, T.H., Didenko, A.N., Johnson, C.L., Khanchuk, A.I., and MacDonald, J.H., Jr., eds., Late Jurassic Margin of Laurasia—A Record of Faulting Accommodating Plate Rotation: Geological Society of America Special Paper 513, p. 107–188, https://doi.org/10.1130/2015.2513(03).

Anfinson, O.A., Leier, A.L., Gaschnig, R., Embry, A.F., and Dewing, K., 2012, U-Pb and Hf isotopic data from Franklinian Basin strata: Insights into the nature of Crockerland and the timing of accretion, Canadian Arctic Islands: Canadian Journal of Earth Sciences, v. 49, p. 1316–1328, https://doi.org/10.1139/e2012-067.

Beranek, L.P., and Mortensen, J.K., 2011, The timing and provenance record of the late Permian Klondike orogeny in northwestern Canada and arc-continent collision along western North America: Tectonics, v. 30, TC5017, https://doi.org/10.1029/2010TC002849.

Beranek, L.P., Mortensen, J.K., Orchard, M.J., and Ullrich, T., 2010, Provenance of North American Triassic strata from west-central and southeastern Yukon: Correlations with coeval strata in the Western Canada Sedimentary Basin and Canadian Arctic Islands: Canadian Journal of Earth Sciences, v. 47, p. 53–73, https://doi.org/10.1139/E09-065.

Beranek, L.P., Link, P.K., and Fanning, C.M., 2016, Detrital zircon record of mid-Paleozoic convergent margin activity in the northern U.S. Rocky Mountains: Implications for the Antler orogeny and early evolution of the North American Cordillera: Lithosphere, v. 8, p. 533–550, https://doi.org/10.1130/L557.1.

Beranek, L.P., McClelland, W.C., van Staal, C.R., Israel, S., and Gordee, S.M., 2017, Late Jurassic flare-up of the Coast Mountains arc system, NW Canada, and dynamic linkages across the northern Cordilleran orogen: Tectonics, v. 36, p. 877–901, https://doi.org/10.1002/2016TC004254.

Beranek, L.P., Gee, D.G., and Fisher, C.M., 2020, Detrital zircon U-Pb-Hf isotope signatures of Old Red Sandstone strata constrain the Silurian to Devonian paleogeography, tectonics, and crustal evolution of the Svalbard Caledonides: Geological Society of America Bulletin, v. 132, p. 1987–2003, https://doi.org/10.1130/B35318.1.

Berman, R.G., Ryan, J.J., Gordey, S.P., and Villeneuve, M., 2007, Permian to Cretaceous polymetamorphic evolution of the Stewart River region, Yukon-Tanana terrane, Yukon, Canada: *P-T* evolution linked with in situ SHRIMP monazite geochronology: Journal of Metamorphic Geology, v. 25, p. 803–827, https://doi.org/10.1111/j.1525-1314.2007.00729.x.

Betka, P.M., Gillis, R.J., and Benowitz, J.A., 2017, Cenozoic sinistral transpression and polyphase slip within the Bruin Bay fault system, Iniskin-Tuxedni region, Cook Inlet, Alaska: Geosphere, v. 13, p. 1806–1833, https://doi.org/10.1130/GES01464.1.

Bickerton, L., Colpron, M., Gibson, H.D., Thorkelson, D.J., and Crowley, J.L., 2020, The northern termination of the Cache Creek terrane in Yukon: Middle Triassic arc activity and Jurassic–Cretaceous structural imbrication: Canadian Journal of Earth Sciences, v. 57, p. 227–248, https://doi.org/10.1139/cjes-2018-0262.

Bordet, E., Crowley, J.L., and Piercey, S.J., 2019, Geology of the Eastern Lake Laberge Area (105E), South-Central Yukon: Yukon Geological Survey Open File 2019–1, 120 p.

Bouvier, A., Vervoort, J.D., and Patchett, P.J., 2008, The Lu-Hf and Sm-Nd isotopic composition of CHUR: Constraints from unequilibrated chondrites and implications for the bulk composition of terrestrial planets: Earth and Planetary Science Letters, v. 273, p. 48–57, https://doi.org/10.1016/j.epsl.2008.06.010.

Calvert, A.J., Hayward, N., Vayavur, R., and Colpron, M., 2017, Seismic and gravity constraints on the crustal architecture of the Intermontane terranes, central Yukon: Canadian Journal of Earth Sciences, v. 54, p. 798–811, https://doi.org/10.1139/cjes-2016-0189.

Canil, D., Mihalynuk, M.G., and Charnell, C., 2006, Sedimentary record for exhumation of ultrahigh pressure (UHP) rocks in the northern Cordillera, British Columbia, Canada: Geological Society of America Bulletin, v. 118, p. 1171–1184, https://doi.org/10.1130/B25921.1.

Cant, D.J., and Stockmal, G.S., 1989, The Alberta foreland basin: Relationship between stratigraphy and Cordilleran terrane-accretion events: Canadian Journal of Earth Sciences, v. 26, p. 1964–1975, https://doi.org/10.1139/e89-166.

Cawood, P.A., Kröner, A., and Collins, W.J., 2009, Accretionary orogens through Earth history, *in* Cawood, P.A., and Kröner, A., eds., Earth Accretionary Systems in Space and Time: Geological Society, London, Special Publication 318, p. 1–36, https://doi.org/10.1144/SP318.1.

Cawood, P.A., Hawkesworth, C.J., and Dhuime, B., 2012, Detrital zircon record and tectonic setting: Geology, v. 40, p. 875–878, https://doi.org/10.1130/G32945.1.

Clark, A.D., 2017, Tectonometamorphic History of Mid-Crustal Rocks at Aishihik Lake, Southwest Yukon [MSc thesis]: Burnaby, British Columbia, Canada, Simon Fraser University, 153 p.

Cohen, K.M., Finney, S.C., Gibbard, P.L., and Fan, J.-X., 2013, The ICS International Chronostratigraphic Chart: Episodes, v. 36, p. 199–204, www.stratigraphy.org (updated December 2021).

Colpron, M., 2011, Geological Compilation of Whitehorse Trough—Whitehorse (105D), Lake Laberge (105E), and Part of Carmacks (115I), Glenlyon (105L), Aishihik Lake (115H), Quiet Lake (105F) and Teslin (105C): Yukon Geological Survey Geoscience Map 2011–1, scale 1:250,000.

Colpron, M., and Friedman, R.M., 2008, U-Pb zircon ages for the Nordenskiöld formation (Laberge Group) and Cretaceous intrusive rocks, Whitehorse trough, Yukon, *in* Emond, D.S., Blackburn, L.R., Hill, R.P., and Weston, L.H., eds., Yukon Exploration and Geology 2007: Whitehorse, Yukon, Canada, Yukon Geological Survey, p. 139–151.

Colpron, M., and Nelson, J.L., 2009, A Palaeozoic Northwest Passage: Incursion of Caledonian, Baltican and Siberian terranes into eastern Panthalassa, and the early evolution of the North American Cordillera, *in* Cawood, P.A., and Kröner, A., eds., Earth Accretionary Systems in Space and Time: Geological Society, London, Special Publication 318, p. 273–307, https://doi.org/10.1144/SP318.10.

Colpron, M., and Ryan, J.J., 2010, Bedrock geology of southwest McQuesten (NTS 115P) and part of northern Carmacks (NTS 115I) map area, *in* MacFarlane, K.E., Weston, L.H., and Blackburn, L.R., eds., Yukon Exploration and Geology 2009: Whitehorse, Yukon, Canada, Yukon Geological Survey, p. 159–184.

Colpron, M., Nelson, J.L., and Murphy, D.C., 2006, A tectonostratigraphic framework for the pericratonic terranes of the northern Cordillera, *in* Colpron, M., and Nelson, J.L., eds., Paleozoic Evolution and Metallogeny of Pericratonic Terranes at the Ancient Pacific Margin of North America, Canadian and Alaskan Cordillera: Geological Association of Canada Special Paper 45, p. 1–23.

Colpron, M., Nelson, J.L., and Murphy, D.C., 2007a, Northern Cordilleran terranes and their interactions through time: GSA Today, v. 17, no. 4/5, p. 4–10, https://doi.org/10.1130/GSAT01704-5A.1.

Colpron, M., Gordey, S.P., Lowey, G.W., White, D., and Piercey, S.J., 2007b, Geology of the Northern Whitehorse Trough, Yukon (NTS 105E/12, 13, and Parts of 11 and 14; 105L/4 and Parts of 3 and 5; Parts of 115H/9 and 16; 115I/1 and Part of 8): Yukon Geological Survey Open-File 2007–6, scale 1:150,000.

Colpron, M., Crowley, J.L., Gehrels, G., Long, D.G.F., Murphy, D.C., Beranek, L., and Bickerton, L., 2015, Birth of the northern Cordilleran orogeny, as recorded by detrital zircons in Jurassic synorogenic strata and regional exhumation in Yukon: Lithosphere, v. 7, p. 541–562, https://doi.org/10.1130/L451.1.

Colpron, M., Sack, P.J., Crowley, J.L., Beranek, L.P., and Allan, M.M., 2022, Late Triassic to Jurassic magmatic and tectonic evolution of the Intermontane terranes in Yukon, northern Canadian Cordillera: Transition from arc to syn-collisional magmatism and post-collisional lithospheric delamination: Tectonics, v. 41, https://doi.org/10.1029/2021TC007060.

Cordey, F., 2020, Timing of Cache Creek Ocean closure: Insights from new Jurassic radiolarian ages in British Columbia and Yukon and their significance for Canadian Cordillera tectonics: Canadian Journal of Earth Sciences, v. 57, p. 1167–1179, https://doi.org/10.1139/cjes-2019-0236.

Coutts, D.S., Matthews, W.A., and Hubbard, S.M., 2019, Assessment of widely used methods to derive depositional ages from detrital zircon populations: Geoscience Frontiers, v. 10, p. 1421–1435, https://doi.org/10.1016/j.gsf.2018.11.002.

Currie, L., and Parrish, R.R., 1993, Jurassic accretion of Nisling terrane along the western margin of Stikinia, Coast Mountains, northwestern British Columbia: Geology, v. 21, p. 235–238, https://doi.org/10.1130/0091-7613(1993)021<0235:JAONTA>2.3.CO;2.

de Keijzer, M., Mihalynuk, M.G., and Johnston, S.T., 2000, Structural Investigation of an Exposure of the Teslin Fault, Northwestern British Columbia: Geological Survey of Canada Current Research 2000–A5, 10 p., https://doi.org/10.4095/211131.

DeCelles, P.G., and Graham, S.A., 2015, Cyclical processes in the North American Cordilleran orogenic system: Geology, v. 43, p. 499–502, https://doi.org/10.1130/G36482.1.

DeCelles, P.G., Ducea, M.N., Kapp, P., and Zandt, G., 2009, Cyclicity in Cordilleran orogenic systems: Nature Geoscience, v. 2, p. 251–257, https://doi.org/10.1038/ngeo469.

Dickie, J.R., and Hein, F.J., 1995, Conglomeratic fan deltas and submarine fans of the Jurassic Laberge Group, Whitehorse trough, Yukon Territory, Canada—Fore-arc sedimentation and unroofing of a volcanic island-arc complex: Sedimentary Geology, v. 98, p. 263–292, https://doi.org/10.1016/0037-0738(95)00036-8.

Dickinson, W.R., 1974, Plate tectonics and sedimentation, *in* Dickinson, W.R., ed., Tectonics and Sedimentation: Society of Economic Paleontologists and Mineralogists (SEPM) Special Publication 22, p. 1–27, https://doi.org/10.2110/pec.74.22.0001.

Dickinson, W.R., and Gehrels, G.E., 2009, Use of U-Pb ages of detrital zircons to infer maximum depositional ages of strata: A test against a Colorado Plateau Mesozoic database: Earth and Planetary Science Letters, v. 288, p. 115–125, https://doi.org/10.1016/j.epsl.2009.09.013.

Dickinson, W.R., and Suczek, C.A., 1979, Plate tectonics and sandstone compositions: American Association of Petroleum Geologists Bulletin, v. 63, p. 2164–2182, https://doi.org/10.1306/2F9188FB-16CE-11D7-8645000102C1865D.

Dickinson, W.R., Beard, L.S., Brakenridge, G.R., Erjavec, J.L., Ferguson, R.C., Inman, K.F., Knepp, R.A., Lindberg, F.A., and Ryberg, P.T., 1983, Provenance of North American Phanerozoic sandstones in relation to tectonic setting: Geological Society of America Bulletin, v. 94, p. 222–235, https://doi.org/10.1130/0016-7606(1983)94<222:PONAPS>2.0.CO;2.

Dostal, J., Keppie, J.D., and Ferri, F., 2009, Extrusion of high-pressure Cache Creek rocks into the Triassic Stikinia-Quesnellia arc of the Canadian Cordillera: Implications for terrane analysis of ancient orogens and palaeogeography, *in* Murphy, J.B., Keppie, J.D., and Hynes, A.J., eds., Ancient Orogens and Modern Analogues: Geological Society, London, Special Publication 327, p. 71–87, https://doi.org/10.1144/SP327.5.

Ducea, M.N., and Barton, M.D., 2007, Igniting flare-up events in Cordilleran arcs: Geology, v. 35, p. 1047–1050, https://doi.org/10.1130/G23898A.1.

Ducea, M.N., Saleeby, J.B., and Bergantz, G., 2015, The architecture, chemistry, and evolution of continental magmatic arcs: Annual Review of Earth and Planetary Sciences, v. 43, p. 299–331, https://doi.org/10.1146/annurev-earth-060614-105049.

Dyer, S., 2020, The Early Jurassic Metamorphic History of the Yukon-Tanana Terrane of Northwestern British Columbia: Insights from a New Inverse Garnet Fractionation Modelling Technique [M.Sc. thesis]: Ottawa, Ontario, Canada, Carleton University, 297 p.

English, J.M., and Johnston, S.T., 2005, Collisional orogenesis in the northern Canadian Cordillera: Implications for Cordilleran crustal structure, ophiolite emplacement, continental growth, and the terrane hypothesis: Earth and Planetary Science Letters, v. 232, p. 333–344, https://doi.org/10.1016/j.epsl.2005.01.025.

Enkelmann, E., Sanchez Lohff, S.K., and Finzel, E.S., 2019, Detrital zircon double-dating of forearc basin strata reveals magmatic, exhumational, and thermal history of sediment source areas: Geological Society of America Bulletin, v. 131, p. 1364–1384, https://doi.org/10.1130/B35043.1.

Fisher, C.M., Vervoort, J.D., and DuFrane, S.A., 2014, Accurate Hf isotopic determinations of complex zircons using the "laser ablation split stream" method: Geochemistry Geophysics Geosystems, v. 15, p. 121–139, https://doi.org/10.1002/2013GC004962.

Flowerdew, M.J., Millar, I.L., Curtis, M.L., Vaughan, A.P.M., Horstwood, M.S.A., Whitehouse, M.J., and Fanning, C.M., 2007, Combined U-Pb geochronology and Hf isotope geochemistry of detrital zircons from early Paleozoic sedimentary rocks, Ellsworth-Whitmore Mountains block, Antarctica: Geological Society of America Bulletin, v. 119, p. 275–288, https://doi.org/10.1130/B25891.1.

Fuentes, F., DeCelles, P.G., and Gehrels, G.E., 2009, Jurassic onset of foreland basin deposition in northwestern Montana, USA: Implications for along-strike synchroneity of Cordilleran orogenic activity: Geology, v. 37, p. 379–382, https://doi.org/10.1130/G25557A.1.

Gagnon, J.-F., Evenchick, C.A., Waldron, J.W.F., Cordey, F., and Poulton, T.P., 2009, Jurassic subsidence history of the Hazelton Trough–Bowser Basin in the area of Todagin Mountain, north-central British Columbia, Canada: Bulletin of Canadian Petroleum Geology, v. 57, p. 430–448, https://doi.org/10.2113/gscpgbull.57.4.430.

Gaidies, F., Morneau, Y.E., Petts, D.C., Jackson, S.E., Zagorevski, A., and Ryan, J.J., 2021, Major and trace element mapping of garnet: Unravelling the conditions, timing and rates of metamorphism of the Snowcap assemblage, west-central Yukon: Journal of Metamorphic Geology, v. 39, p. 133–164, https://doi.org/10.1111/jmg.12562.

Gehrels, G.E., 2001, Geology of the Chatham Sound region, southeast Alaska and coastal British Columbia: Canadian Journal of Earth Sciences, v. 38, p. 1579–1599, https://doi.org/10.1139/e01-040.

Gehrels, G.E., Rusmore, M., Woodsworth, G.J., Crawford, M., Andronicos, C., Hollister, L., Patchett, P.J., Ducea, M., Butler, R.F., Klepeis, K., Davidson, C., Friedman, R.M., Haggart, J., Mahoney, J.J., Crawford, W., Pearson, D., and Girardi, J., 2009, U-Th-Pb geochronology of the Coast Mountains batholith in north-coastal British Columbia: Constraints on age and tectonic evolution: Geological Society of America Bulletin, v. 121, p. 1341–1361, https://doi.org/10.1130/B26404.1.

George, S.W.M., Nelson, J.L., Alberts, D., Greig, C.J., and Gehrels, G.E., 2021, Triassic–Jurassic accretionary history and tectonic origins of Stikinia from U-Pb geochronology and Lu-Hf isotope analysis, British Columbia: Tectonics, v. 40, https://doi.org/10.1029/2020TC006505.

Golding, M.L., Mortensen, J.K., Zonneveld, J.-P., and Orchard, M.J., 2016, U-Pb isotopic ages of euhedral zircons in the Rhaetian of British Columbia: Implications for Cordilleran tectonics during the Late Triassic: Geosphere, v. 12, p. 1606–1616, https://doi.org/10.1130/GES01324.1.

Goodge, J.W., and Vervoort, J.D., 2006, Origin of Mesoproterozoic A-type granites in Laurentia: Hf isotopic evidence: Earth and Planetary Science Letters, v. 243, p. 711–731, https://doi.org/10.1016/j.epsl.2006.01.040.

Gordey, S.P., McNicoll, V.J., and Mortensen, J.K., 1998, New U-Pb ages from the Teslin area, southern Yukon, and their bearing on terrane evolution in the northern Cordillera, *in* Radiogenic Age and Isotopic Studies Report 11: Geological Survey of Canada Current Research 1998-F, p. 129–148, https://doi.org/10.4095/210064.

Gunning, M.H., Hodder, R.W.H., and Nelson, J.L., 2006, Contrasting volcanic styles and their tectonic implications for the Paleozoic Stikine assemblage, western Stikine terrane, northwestern British Columbia, *in* Colpron, M., and Nelson, J.L., eds., Paleozoic Evolution and Metallogeny of Pericratonic Terranes at the Ancient Pacific Margin of North America, Canadian and Alaskan Cordillera: Geological Association of Canada Special Paper 45, p. 201–227.

Hall, R., McNicoll, V., Gröcke, D., Craig, J., and Johnston, K., 2004, Integrated stratigraphy of the lower and middle Fernie Formation in Alberta and British Columbia, western Canada: Rivista Italiana di Paleontologia e Stratigrafia, v. 110, p. 61–68, https://doi.org/10.13130/2039-4942/6264.

Hart, C.J.R., 1997, A Transect across Northern Stikinia: Geology of the Northern Whitehorse Map Area, Southern Yukon Territory (105D/13–16): Exploration and Geological Services Division, Yukon Region, Indian and Northern Affairs Canada, Bulletin 8, 112 p.

Hart, C.J.R., and Radloff, J.K., 1990, Geology of Whitehorse, Alligator Lake, Fenwick Creek, Carcross and Part of Robinson Map Areas (105D/11, 6, 3, 2 & 7): Yukon Geological Survey Open-File 1990–4(G), scale 1:50,000.

Hart, C.J.R., Dickie, J.R., Ghosh, D.K., and Armstrong, R.L., 1995, Provenance constraints for Whitehorse trough conglomerate: U-Pb zircon dates and initial Sr ratios of granitic clasts in Jurassic Laberge Group, Yukon Territory, *in* Miller, D.M., and Busby, C., eds., Jurassic Magmatism and Tectonics of the North American Cordillera: Geological Society of America Special Paper 299, p. 47–64, https://doi.org/10.1130/SPE299-p47.

Hawkesworth, C.J., and Kemp, A.I.S., 2006, Using hafnium and oxygen isotopes in zircons to unravel the record of crustal evolution: Chemical Geology, v. 226, p. 144–162, https://doi.org/10.1016/j.chemgeo.2005.09.018.

Herriott, T.M., Crowley, J.L., Schmitz, M.D., Wartes, M.A., and Gillis, R.J., 2019, Exploring the law of detrital zircon: LA-ICP-MS and CA-TIMS geochronology of Jurassic forearc strata, Cook Inlet, Alaska, USA: Geology, v. 47, p. 1044–1048, https://doi.org/10.1130/G46312.1.

Horton, B.K., 2018, Sedimentary record of Andean mountain building: Earth-Science Reviews, v. 178, p. 279–309, https://doi.org/10.1016/j.earscirev.2017.11.025.

Horton, B.K., Saylor, J.E., Nie, J., Mora, A., Parra, M., Reyes-Harker, A., and Stockli, D.F., 2010, Linking sedimentation in the northern Andes to basement configuration, Mesozoic extension, and Cenozoic shortening: Evidence from detrital zircon U-Pb ages, Eastern Cordillera, Colombia: Geological Society of America Bulletin, v. 122, p. 1423–1442, https://doi.org/10.1130/B30118.1.

Hutchison, M.P., 2017, Whitehorse Trough: Past, Present and Future Petroleum Research, with a Focus on Reservoir Characterization of the Northern Laberge Group: Yukon Geological Survey Open File 2017–2, 48 p.

Hutter, A.D., and Beranek, L.P., 2020, Provenance of Upper Jurassic to Lower Cretaceous synrift strata in the Terra Nova oil field, Jeanne d'Arc basin, offshore Newfoundland: A new detrital zircon U-Pb-Hf reference frame for the Atlantic Canadian margin: American Association of Petroleum Geologists Bulletin, v. 104, p. 2325–2349, https://doi.org/10.1306/02232018241.

Iizuka, T., Komiya, T., Rino, S., Maruyama, S., and Hirata, T., 2010, Detrital zircon evidence for Hf isotopic evolution of granitoid crust and continental growth: Geochimica et Cosmochimica Acta, v. 74, p. 2450–2472, https://doi.org/10.1016/j.gca.2010.01.023.

Ingersoll, R.V., Kretchmer, A.G., and Valles, P.K., 1993, The effect of sampling scale on actualistic sandstone petrofacies: Sedimentology, v. 40, p. 937–953, https://doi.org/10.1111/j.1365-3091.1993.tb01370.x.

Johannson, G.G., Smith, P.L., and Gordey, S.P., 1997, Early Jurassic evolution of the northern Stikinian arc: Evidence from the Laberge Group, northwestern British Columbia: Canadian Journal of Earth Sciences, v. 34, p. 1030–1057, https://doi.org/10.1139/e17-085.

Johnsson, M.J., 1993, The system controlling the composition of clastic sediments, *in* Johnsson, M.J., and Basu, A., eds., Processes Controlling the Composition of Clastic Sediments: Geological Society of America Special Paper 284, p. 1–20, https://doi.org/10.1130/SPE284-p1.

Johnston, S.T., and Erdmer, P., 1995, Hot-side-up aureole in southwest Yukon and limits on terrane assembly of the northern Canadian Cordillera: Geology, v. 23, p. 419–422, https://doi.org/10.1130/0091-7613(1995)023<0419:HSUAIS>2.3.CO;2.

Johnston, S.T., Mortensen, J.K., and Erdmer, P., 1996, Igneous and metaigneous age constraints for the Aishihik metamorphic suite, southwest Yukon: Canadian Journal of Earth Sciences, v. 33, p. 1543–1555, https://doi.org/10.1139/e96-117.

Kellett, D.A., and Iraheta Muniz, P., 2019, Detrital U-Pb Zircon and $^{40}Ar/^{39}Ar$ Muscovite Geochronology of the Whitehorse Trough, and Surrounding Rocks, Yukon and British Columbia: Geological Survey of Canada Open-File 8565, 35 p., https://doi.org/10.4095/314694.

Kellett, D.A., and Zagorevski, A., 2021, Overlap assemblages: Laberge Group of the Whitehorse trough, northern Canadian Cordillera, Yukon–British Columbia, *in* Ryan, J.J., and Zagorevski, A., eds., Northern Cordillera Geology: A Synthesis of Research from the Geo-Mapping for Energy and Minerals Program, British Columbia and Yukon: Geological Survey of Canada Bulletin 610, p. 1–22.

Kellett, D.A., Weller, O.M., Zagorevski, A., and Regis, D., 2018, A petrochronological approach for the detrital record: Tracking mm-sized eclogite clasts in the northern Canadian Cordillera: Earth and Planetary Science Letters, v. 494, p. 23–31, https://doi.org/10.1016/j.epsl.2018.04.036.

Knight, E., Schneider, D.A., and Ryan, J., 2013, Thermochronology of the Yukon-Tanana terrane, west-central Yukon: Evidence for Jurassic extension and exhumation in the northern Canadian Cordillera: The Journal of Geology, v. 121, p. 371–400, https://doi.org/10.1086/670721.

LaMaskin, T., Dorsey, R.J., Vervoort, J.D., Schmitz, M.D., Tumpane, K.P., and Moore, N.O., 2015, Westward growth of Laurentia by pre–Late Jurassic terrane accretion, eastern Oregon and western Idaho, United States: The Journal of Geology, v. 123, p. 233–267, https://doi.org/10.1086/681724.

Laskowski, A.K., DeCelles, P.G., and Gehrels, G.E., 2013, Detrital zircon geochronology of Cordilleran retroarc foreland basin strata, western North America: Tectonics, v. 32, p. 1027–1048, https://doi.org/10.1002/tect.20065.

Link, P.K., Fanning, C.M., and Beranek, L.P., 2005, Reliability and longitudinal change of detrital-zircon age spectra in the Snake River system, Idaho and Wyoming: An example of reproducing the bumpy barcode: Sedimentary Geology, v. 182, p. 101–142, https://doi.org/10.1016/j.sedgeo.2005.07.012.

Liu, X.-C., Wu, Y.-B., Fisher, C.M., Hanchar, J.M., Beranek, L., Gao, S., and Wang, H., 2017, Tracing crustal evolution by U-Th-Pb, Sm-Nd, and Lu-Hf isotopes in detrital monazite and zircon from modern rivers: Geology, v. 45, p. 103–106, https://doi.org/10.1130/G38720.1.

Logan, J.M., Drobe, J.R., and McClelland, W.C., 2000, Geology of the Forrest Kerr–Mess Creek Area, Northwestern British Columbia (NTS 104B/10, 15 & 104G/2 & 7W): British Columbia Ministry of Energy and Mines Bulletin 104, 164 p.

Long, D.G.F., 1986, Coal in Yukon, *in* Morin, J.A., ed., Mineral Deposits of the Northern Cordillera: Canadian Institute of Mining and Metallurgy Special Volume 37, p. 311–318.

Long, D.G.F., 2005, Sedimentology and hydrocarbon potential of fluvial strata in the Tantalus and Aksala formations, northern Whitehorse trough, Yukon, *in* Emond, D.S., Lewis, L.L., and Bradshaw, G.D., eds., Yukon Exploration and Geology 2004: Whitehorse, Yukon, Canada, Yukon Geological Survey, p. 167–176.

Long, D.G.F., 2015, Depositional and Tectonic Framework of Braided and Meandering Gravel-Bed River Deposits and Associated Coal Deposits in Active Intermontane Basins: The Upper Jurassic to Mid-Cretaceous Tantalus Formation, Whitehorse Trough, Yukon, Canada: Yukon Geological Survey Open-File 2015–23, 80 p.

Lowey, G.W., 2004, Preliminary lithostratigraphy of the Laberge Group (Jurassic), south-central Yukon: Implications concerning the petroleum potential of the Whitehorse trough, *in* Emond, D.S., and Lewis, L.L., eds., Yukon Exploration and Geology 2003: Whitehorse, Yukon, Canada, Yukon Geological Survey, p. 129–142.

Lowey, G.W., 2008, Summary of the stratigraphy, sedimentology and hydrocarbon potential of the Laberge Group (Lower–Middle Jurassic), Whitehorse trough, Yukon, *in* Emond, D.S.,

Blackburn, L.R., Hill, R.P., and Weston, L.H., eds., Yukon Exploration and Geology 2007: Whitehorse, Yukon, Canada, Yukon Geological Survey, p. 179–197.
McClelland, W.C., and Gehrels, G.E., 1990, Geology of the Duncan Canal shear zone: Evidence for Early to Middle Jurassic deformation of the Alexander terrane, southeastern Alaska: Geological Society of America Bulletin, v. 102, p. 1378–1392, https://doi.org/10.1130/0016-7606(1990)102<1378:GOTDCS>2.3.CO;2.
McClelland, W.C., Gehrels, G.E., and Saleeby, J.B., 1992, Upper Jurassic–Lower Cretaceous basinal strata along the Cordilleran margin: Implications for the accretionary history of the Alexander-Wrangellia-Peninsular terrane: Tectonics, v. 11, p. 823–835, https://doi.org/10.1029/92TC00241.
Mihalynuk, M.G., Nelson, J., and Diakow, L.J., 1994, Cache Creek terrane entrapment: Oroclinal paradox within the Canadian Cordillera: Tectonics, v. 13, p. 575–595, https://doi.org/10.1029/93TC03492.
Mihalynuk, M.G., Mountjoy, K.J., Smith, M.T., Currie, L.D., Gabites, J.E., Tipper, H.W., Orchard, M.J., Poulton, T.P., and Cordey, F., 1999, Geology and Mineral Resources of the Tagish Lake Area (NTS 104M/8, 9, 10E, 15 and 104N/12W), Northwestern British Columbia: British Columbia Ministry of Energy and Mines Bulletin 105, 217 p.
Mihalynuk, M.G., Erdmer, P., Ghent, E.D., Cordey, F., Archibald, D.A., Friedman, R.M., and Johannson, G.G., 2004, Coherent French Range blueschist: Subduction to exhumation in <2.5 m.y.?: Geological Society of America Bulletin, v. 116, p. 910–922, https://doi.org/10.1130/B25393.1.
Monger, J.W.H., and Gibson, H.D., 2019, Mesozoic–Cenozoic deformation in Canadian Cordillera: The record of a "continental bulldozer"?: Tectonophysics, v. 757, p. 153–169, https://doi.org/10.1016/j.tecto.2018.12.023.
Monger, J.W.H., and Price, R., 2002, The Canadian Cordillera: Geology and tectonic evolution: Canadian Society of Exploration Geophysicists Recorder, v. 27, p. 17–36.
Mortensen, J.K., 1992, Pre–mid-Mesozoic tectonic evolution of the Yukon-Tanana terrane, Yukon and Alaska: Tectonics, v. 11, p. 836–853, https://doi.org/10.1029/91TC01169.
Murphy, D.C., van der Heyden, P., Parrish, R.R., Klepacki, D.W., McMillan, W., Struik, L.C., and Gabites, J., 1995, New geochronological constraints on Jurassic deformation of the western edge of North America, southeastern Canadian Cordillera, *in* Miller, D.M., and Busby, C., eds., Jurassic Magmatism and Tectonics of the North American Cordillera: Geological Society of America Special Paper 299, p. 159–172, https://doi.org/10.1130/SPE299-p159.
Murphy, D.C., Mortensen, J.K., Piercey, S.J., Orchard, M.J., and Gehrels, G.E., 2006, Mid-Paleozoic to early Mesozoic tectonostratigraphic evolution of Yukon-Tanana and Slide Mountain terranes and affiliated overlap assemblages, Finlayson Lake massive sulphide district, southeastern Yukon, *in* Colpron, M., and Nelson, J.L., eds., Paleozoic Evolution and Metallogeny of Pericratonic Terranes at the Ancient Pacific Margin of North America, Canadian and Alaskan Cordillera: Geological Association of Canada Special Paper 45, p. 75–105.
Nelson, J., and Mihalynuk, M., 1993, Cache Creek ocean: Closure or enclosure?: Geology, v. 21, p. 173–176, https://doi.org/10.1130/0091-7613(1993)021<0173:CCOCOE>2.3.CO;2.
Nelson, J.L., and Friedman, R.M., 2004, Superimposed Quesnel (late Paleozoic–Jurassic) and Yukon-Tanana (Devonian–Mississippian) arc assemblages, Cassiar Mountains, northern British Columbia: Field, U-Pb and igneous petrochemical evidence: Canadian Journal of Earth Sciences, v. 41, p. 1201–1235, https://doi.org/10.1139/e04-028.
Nelson, J.L., Colpron, M., Piercey, S.J., Dusel-Bacon, C., Murphy, D.C., and Roots, C.F., 2006, Paleozoic tectonic and metallogenic evolution of the pericratonic terranes in Yukon, northern British Columbia and eastern Alaska, *in* Colpron, M., and Nelson, J.L., eds., Paleozoic Evolution and Metallogeny of Pericratonic Terranes at the Ancient Pacific Margin of North America, Canadian and Alaskan Cordillera: Geological Association of Canada Special Paper 45, p. 323–360.
Nelson, J.L., Colpron, M., and Israel, S., 2013, The Cordillera of British Columbia, Yukon, and Alaska: Tectonics and metallogeny, *in* Colpron, M., Bissig, T., Rusk, B.G., and Thompson, J.F.H., eds., Tectonics, Metallogeny and Discovery: The North American Cordillera and Similar Accretionary Settings: Society of Economic Geologists Special Publication 17, p. 53–103, https://doi.org/10.5382/SP.17.03.
Nelson, J.L., van Straaten, B., and Friedman, R., 2022, Latest Triassic–Early Jurassic Stikine–Yukon-Tanana terrane collision and the onset of accretion in the Canadian Cordillera: Insights from Hazelton Group detrital zircon provenance and volcano-sedimentary facies architecture: Geosphere, v. 18, p. 670–696, https://doi.org/10.1130/GES02444.1.
Nixon, G.T., Scheel, J.E., Scoates, J.S., Friedman, R.M., Wall, C.J., Gabites, J., and Jackson-Brown, S., 2020, Syn-accretionary multistage assembly of an Early Jurassic Alaskan-type intrusion in the Canadian Cordillera: U-Pb and ^{40}Ar-^{39}Ar geochronology of the Turnagain ultramafic-mafic intrusive complex, Yukon-Tanana terrane: Canadian Journal of Earth Sciences, v. 57, p. 575–600, https://doi.org/10.1139/cjes-2019-0121.
Pană, D.I., Poulton, T.P., and DuFrane, S.A., 2019, U-Pb detrital zircon dating supports Early Jurassic initiation of the Cordilleran foreland basin in southwestern Canada: Geological Society of America Bulletin, v. 131, p. 318–334, https://doi.org/10.1130/B31862.1.
Paton, C., Woodhead, J.D., Hellstrom, J.C., Hergt, J.M., Greig, A., and Maas, R., 2010, Improved laser ablation U-Pb zircon geochronology through robust downhole fractionation correction: Geochemistry, Geophysics, Geosystems, v. 11, Q0AA06, https://doi.org/10.1029/2009GC002618.
Pearce, J.A., Harris, N.B.W., and Tindle, A.G., 1984, Trace element discrimination diagrams for the tectonic interpretation of granitic rocks: Journal of Petrology, v. 25, p. 956–983, https://doi.org/10.1093/petrology/25.4.956.
Pecha, M.E., Gehrels, G.E., McClelland, W.C., Giesler, D., White, C., and Yokelson, I., 2016, Detrital zircon U-Pb geochronology and Hf isotope geochemistry of the Yukon-Tanana terrane, Coast Mountains, southeast Alaska: Geosphere, v. 12, no. 5, p. 1556–1574, https://doi.org/10.1130/GES01303.1.
Pepper, M., Gehrels, G.E., Pullen, A., Ibanez-Mejia, M., Ward, K.M., and Kapp, P., 2016, Magmatic history and crustal genesis of western South America: Constraints from U-Pb ages and Hf isotopes of detrital zircons in modern rivers: Geosphere, v. 12, p. 1532–1555, https://doi.org/10.1130/GES01315.1.
Petrus, J.A., and Kamber, B.S., 2012, VizualAge: A novel approach to laser ablation ICP-MS U-Pb geochronology data reduction: Geostandards and Geoanalytical Research, v. 36, p. 247–270, https://doi.org/10.1111/j.1751-908X.2012.00158.x.
Piercey, S.J., and Colpron, M., 2009, Composition and provenance of the Snowcap assemblage, basement to the Yukon-Tanana terrane, northern Cordillera: Implications for Cordilleran crustal growth: Geosphere, v. 5, p. 439–464, https://doi.org/10.1130/GES00505.1.
Piercey, S.J., Nelson, J.L., Colpron, M., Dusel-Bacon, C., Simard, R.-L., and Roots, C.F., 2006, Paleozoic magmatism and crustal recycling along the ancient Pacific margin of North America, northern Canadian Cordillera, *in* Colpron, M., and Nelson, J.L., eds., Paleozoic Evolution and Metallogeny of Pericratonic Terranes at the Ancient Pacific Margin of North America, Canadian and Alaskan Cordillera: Geological Association of Canada Special Paper 45, p. 281–322.
Poulton, T.P., 1989, Upper Absaroka to lower Zuni: The transition to the foreland basin, *in* Ricketts, B.D., ed., Western Canada Sedimentary Basin: A Case History: Canadian Society of Petroleum Geologists Special Publication 30, p. 233–247.
Price, R.A., 1994, Cordilleran tectonics and the evolution of the Western Canada sedimentary basin, *in* Mossop, G., and Shestin, I., eds., Geologic Atlas of the Western Canada Sedimentary Basin: Calgary, Alberta, Canada, Alberta Research Council and Canadian Society of Petroleum Geologists, p. 13–24.
Romero, M.C., Ridgway, K.D., and Gehrels, G.E., 2020, Geology, U-Pb geochronology, and Hf isotope geochemistry across the Mesozoic Alaska Range suture zone (south-central Alaska): Implications for Cordilleran collisional processes and tectonic growth of North America: Tectonics, v. 39, https://doi.org/10.1029/2019TC005946.
Roots, C.F., Nelson, J.L., Simard, R.-L., and Harms, T.A., 2006, Continental fragments, mid-Paleozoic arcs and overlapping late Paleozoic arc and Triassic sedimentary strata in the Yukon-Tanana terrane of northern British Columbia and southern Yukon, *in* Colpron, M., and Nelson, J.L., eds., Paleozoic Evolution and Metallogeny of Pericratonic Terranes at the Ancient Pacific Margin of North America, Canadian and Alaskan Cordillera: Geological Association of Canada Special Paper 45, p. 153–177.
Sack, P.J., Colpron, M., Crowley, J.L., Ryan, J.J., Allan, M.M., Beranek, L.P., and Joyce, N.L., 2020, Atlas of Late Triassic to Jurassic Plutons in the Intermontane Terranes of Yukon: Yukon Geological Survey Open-File 2020–1, 365 p.
Saylor, J.E., and Sundell, K.E., 2016, Quantifying comparison of large detrital geochronology data sets: Geosphere, v. 12, p. 203–220, https://doi.org/10.1130/GES01237.1.
Saylor, J.E., Jordan, J.C., Sundell, K.E., Wang, X., Wang, S., and Deng, T., 2018, Topographic growth of the Jishi Shan and its impact on basin and hydrology evolution, NE Tibetan Plateau: Basin Research, v. 30, p. 544–563, https://doi.org/10.1111/bre.12264.
Shirmohammad, F., Smith, P.L., Anderson, R.G., and McNicoll, V.J., 2011, The Jurassic succession at Lisadele Lake (Tulsequah map area, British Columbia, Canada) and its bearing on the tectonic evolution of the Stikine terrane: Volumina Jurassica, v. 9, p. 43–60.
Simard, R.-L., and Devine, F., 2003, Preliminary geology of the southern Semenof Hills, central Yukon (105E/1,7,8), *in* Emond, D.S., and Lewis, L.L., eds., Yukon Exploration and Geology 2002: Whitehorse, Yukon, Canada, Yukon Geological Survey, p. 213–222.
Simard, R.-L., Dostal, J., and Roots, C.F., 2003, Development of late Paleozoic volcanic arcs in the Canadian Cordillera: An example from the Klinkit Group, northern British Columbia and

southern Yukon: Canadian Journal of Earth Sciences, v. 40, p. 907–924, https://doi.org/10.1139/e03-025.
Sláma, J., Košler, J., Condon, D.J., Crowley, J.L., Gerdes, A., Hanchar, J.M., Horstwood, M.S.A., Morris, G.A., Nasdala, L., Norberg, N., Schaltegger, U., Schoene, B., Tubrett, M.N., and Whitehouse, M.J., 2008, Plešovice zircon—A new natural reference material for U-Pb and Hf isotopic microanalysis: Chemical Geology, v. 249, p. 1–35, https://doi.org/10.1016/j.chemgeo.2007.11.005.
Söderlund, U., Patchett, P.J., Vervoort, J.D., and Isachsen, C.E., 2004, The ^{176}Lu decay constant determined by Lu-Hf and U-Pb isotope systematics of Precambrian mafic intrusions: Earth and Planetary Science Letters, v. 219, p. 311–324, https://doi.org/10.1016/S0012-821X(04)00012-3.
Tempelman-Kluit, D.J., 1984, Geology, Laberge (105E) and Carmacks (105I), Yukon Territory: Geological Survey of Canada Open-File 1101, scale 1:250,000.
Tempelman-Kluit, D.J., 2009, Geology of Carmacks and Laberge Map Areas, Central Yukon: Incomplete Draft Manuscript on Stratigraphy, Structure and its Early Interpretation (ca. 1986): Geological Survey of Canada Open-File 5982, 399 p.
Trop, J.M., and Ridgway, K.D., 2007, Mesozoic and Cenozoic tectonic growth of southern Alaska: A sedimentary basin perspective, *in* Ridgway, K.D., Trop, J.M., Glen, J.M.G., and O'Neill, J.M., eds., Tectonic Growth of a Collisional Continental Margin: Crustal Evolution of Southern Alaska: Geological Society of America Special Paper 431, p. 55–94, https://doi.org/10.1130/2007.2431(04).
Trop, J.M., Szuch, D.A., Rioux, M., and Blodgett, R.B., 2005, Sedimentology and provenance of the Upper Jurassic Naknek Formation, Talkeetna Mountains, Alaska: Bearings of the accretionary tectonic history of the Wrangellia composite terrane: Geological Society of America Bulletin, v. 117, p. 570–588, https://doi.org/10.1130/B25575.1.
Unterschutz, J.L.E., Creaser, R.A., Erdmer, P., Thompson, R.I., and Daughtry, K.L., 2002, North American margin origin of Quesnel terrane strata in the southern Canadian Cordillera: Inferences from geochemical and Nd isotopic characteristics of Triassic metasedimentary rocks: Geological Society of America Bulletin, v. 114, p. 462–475, https://doi.org/10.1130/0016-7606(2002)114<0462:NAMOOQ>2.0.CO;2.
van der Heyden, P., 1992, A Middle Jurassic to early Tertiary Andean-Sierran arc model for the Coast belt of British Columbia: Tectonics, v. 11, p. 82–97, https://doi.org/10.1029/91TC02183.
van Drecht, L.H., and Beranek, L.P., 2018, New investigations of basal Laberge Group stratigraphy, Whitehorse trough, central Yukon, *in* MacFarlane, K.E., ed., Yukon Exploration and Geology 2017: Whitehorse, Yukon, Canada, Yukon Geological Survey, p. 151–163.
van Drecht, L.H., Beranek, L.P., and Hutchison, H., 2017, Jurassic stratigraphy and tectonic evolution of the Whitehorse trough, central Yukon: Project outline and preliminary field results, *in* MacFarlane, K.E., and Weston, L.H., eds., Yukon Exploration and Geology 2016: Whitehorse, Yukon, Canada, Yukon Geological Survey, p. 207–223.
Vervoort, J.D., and Blichert-Toft, J., 1999, Evolution of the depleted mantle: Hf isotope evidence from juvenile rocks through time: Geochimica et Cosmochimica Acta, v. 63, p. 533–556, https://doi.org/10.1016/S0016-7037(98)00274-9.
Wernicke, B., and Klepacki, D.W., 1988, Escape hypothesis for the Stikine block: Geology, v. 16, p. 461–464, https://doi.org/10.1130/0091-7613(1988)016<0461:EHFTSB>2.3.CO;2.
Wheeler, J.O., 1961, Whitehorse Map Area, Yukon Territory, 105D: Ottawa, Ontario, Canada, Geological Survey of Canada Memoir 312, 156 p., https://doi.org/10.4095/100539.
White, D., Colpron, M., and Buffett, G., 2012, Seismic and geological constraints on the structure of the northern Whitehorse trough, Yukon, Canada: Bulletin of Canadian Petroleum Geology, v. 60, p. 239–255, https://doi.org/10.2113/gscpgbull.60.4.239.
Wiedenbeck, M., Allé, P., Griffin, W.L., Meier, M., Oberli, F., von Quadt, A., Roddick, J.C., and Spiegel, W., 1995, Three natural zircon standards for U-Th-Pb, Lu-Hf, trace element and REE analyses: Geostandards Newsletter, v. 19, p. 1–23, https://doi.org/10.1111/j.1751-908X.1995.tb00147.x.
Willner, A.P., Gerdes, A., and Massonne, H.-J., 2008, History of crustal growth and recycling at the Pacific convergent margin of South America at latitudes 29°–36°S revealed by a U-Pb and Lu-Hf isotope study of detrital zircon from late Paleozoic accretionary systems: Chemical Geology, v. 253, p. 114–129, https://doi.org/10.1016/j.chemgeo.2008.04.016.
Wu, F.-Y., Ji, W.-Q., Liu, C.-Z., and Chung, S.-L., 2010, Detrital zircon U-Pb and Hf isotopic data from the Xigaze fore-arc basin: Constraints on Transhimalayan magmatic evolution in southern Tibet: Chemical Geology, v. 271, p. 13–25, https://doi.org/10.1016/j.chemgeo.2009.12.007.
Zagorevski, A., Soucy La Roche, R., Golding, M.L., Joyce, N.L., Regis, D., and Coleman, M., 2018, Stikinia Bedrock, British Columbia and Yukon: GEM-2 Cordillera Project, Report of Activities 2018: Geological Survey of Canada Open-File 8485, 12 p., https://doi.org/10.4095/311325.
Zagorevski, A., van Staal, C.R., Bédard, J.H., Bogatu, A., Canil, D., Coleman, M., Golding, M.L., Joyce, N.L., Lawley, C., McGoldrick, S., Mihalynuk, M.G., Milidragovic, D., Parsons, A.J., and Schiarizza, P., 2021, Overview of Cordilleran oceanic terranes and their significance for the tectonic evolution of the northern Cordillera, *in* Ryan, J.J., and Zagorevski, A., eds., Northern Cordillera Geology: A Synthesis of Research from the Geo-Mapping for Energy and Minerals Program, British Columbia and Yukon: Geological Survey of Canada Bulletin 610, p. 21–65.